Spatial Transcriptomic Analysis Identifies Epithelium-Macrophage Crosstalk in Endometriotic Lesions

Gregory W. Burns[1], Zhen Fu[2], Erin L. Vegter[1], Zachary B. Madaj[2], Erin Greaves[3], Idhaliz Flores[4], and Asgerally T. Fazleabas[1]*

[1]Department of Obstetrics, Gynecology and Reproductive Biology, Michigan State University, Grand Rapids, MI, USA

[2]Bioinformatics and Biostatistics, Van Andel Institute, Grand Rapids, MI, USA

[3]Division of Biomedical Sciences, University of Warwick, Coventry, UK

[4]Department of Basic Sciences, Ponce Research Institute, Ponce Health Sciences University, Ponce, PR, USA

*Corresponding author
Email: fazleaba@msu.edu
Address: 400 Monroe Ave NW, GRRC 3020, Grand Rapids, MI 49503 USA
Telephone: +1 616-234-0981

Abstract

The mechanisms underlying the pathophysiology of endometriosis, characterized by the presence of endometrium-like tissue outside the uterus, remain poorly understood. This study aimed to identify cell type-specific gene expression changes in superficial peritoneal endometriotic lesions and elucidate the crosstalk among the stroma, epithelium, and macrophages compared to patient-matched eutopic endometrium. Surprisingly, comparison between lesions and eutopic endometrium revealed transcriptional similarities, indicating minimal alterations in the sub-epithelial stroma and epithelium of lesions. Spatial transcriptomics highlighted increased signaling between the lesion epithelium and macrophages, emphasizing the role of the epithelium in driving lesion inflammation. We propose that the superficial endometriotic lesion epithelium orchestrates inflammatory signaling and promotes a pro-repair phenotype in macrophages, providing a new role for Complement 3 in lesion pathobiology. This study underscores the significance of considering spatial context and cellular interactions in uncovering mechanisms governing disease in endometriotic lesions.

Introduction

Endometriosis affects around 10% of reproductive age women and is defined by the presence of endometrium-like tissue growing outside of the uterus [1-3]. The disease is clinically associated with life-altering pain and infertility and up to 50% of infertile women are diagnosed with endometriosis [4, 5]. Endometriotic lesions are estrogen-dependent and the only effective non-surgical treatment is suppression of ovarian function to limit estrogen production. Endometriotic lesions in the peritoneal cavity are classified by location with lesions present on the visceral or parietal peritoneum termed peritoneal lesions and those on the ovary termed endometriomas. Peritoneal lesions are further separated into superficial or deep infiltrating according to the invasion depth of underlying tissue with deep infiltrating lesions invading more than 5 mm [6, 7]. Superficial peritoneal endometriotic lesions likely develop from endometrial tissue fragments that are refluxed into the peritoneal cavity during menstruation [8, 9]. This hypothesis is supported by the baboon model of endometriosis in which menstrual tissue inoculated into the peritoneal cavity results in endometriotic lesions and disease that persists for at least 15 months [10-12]. Endometriosis can also be induced in mice with tissue collected from an artificial menstruation cycle [13, 14].

Superficial peritoneal lesions generally consist of endometrium-like epithelium and stroma, fibroblasts that express smooth muscle actin (ACTA2), and immune cells [15]. The presence of ACTA2+ fibroblasts is positively correlated with fibrotic lesions where the presence of epithelium is less common, in contrast to lesions of endometrium-like stroma and epithelium [16, 17]. During lesion development, activation of pro-inflammatory immune populations, specifically macrophages, provide a hospitable inflammatory environment to protect the ectopic endometrial tissue [18]. Previous bulk and single-cell RNA-sequencing analyses have uncovered thousands of differentially expressed genes (DEG) in endometriotic lesions, notably including inflammation- and immune-related genes [19-23]. While bulk RNA-sequencing offers

54 comprehensive data, it lacks the ability to discern information about individual cell types.
55 Conversely, single-cell RNA-sequencing provides insights into cell type-specific expression but
56 relies on post-hoc cell type identification using known markers and lacks spatial context. The
57 emergence of spatial transcriptomics has addressed these limitations by providing a powerful tool
58 to understand the spatial context of gene expression within tissues, particularly when coupled
59 with canonical cell type immunostaining. Two of the most prominent platforms for spatial
60 transcriptomics, NanoString GeoMx and 10X Visium, offer distinct advantages and limitations
61 depending on experimental design. In this study, we chose the GeoMx platform based on the
62 ability to provide cell type specific data from formalin fixed paraffin embedded (FFPE) tissues with
63 high specificity based on antibody-based fluorescent segmentation [24-26]. Our aim was to
64 determine the genes and pathways altered in the glandular epithelium, stroma, and macrophages
65 within endometriotic lesions compared to matched endometrium with spatial transcriptomics. We
66 hypothesized that gene expression changes in superficial peritoneal endometriotic lesions would
67 manifest in a cell type-specific manner, with disruption of the crosstalk among the stroma,
68 epithelium, and macrophages being evident compared to patient-matched eutopic endometrium.

69 Results

70 Spatial Transcriptomics of Human Superficial Peritoneal Lesions

71 We sought to determine the contributions of epithelium, stroma, and myeloid cell
72 compartments of endometriotic lesions to altered genes and pathways in endometriotic lesions
73 by spatial transcriptomic analyses. Superficial peritoneal lesions and eutopic uterine tissue were
74 collected from women in the secretory phase of the menstrual cycle. Matched lesion and eutopic
75 tissues from five women (n = 10) were selected based on the histological presence of endometrial
76 gland-like structures in lesions confirmed by trichrome staining (Figure 1). The average age of the
77 patients was 42 (Table 1, SD = 6.1). Tissues were stained for pan-cytokeratin, smooth muscle

actin, and CD68 to identify epithelium (pan-cytokeratin+), stroma (ACTA2) and myeloid-lineage cells (CD68+, monocytes and macrophages). Myeloid cells were present in both eutopic endometrium and endometriotic lesions within stromal and epithelial compartments (Figure 1). ACTA2+ cells were present in the vasculature and stroma, although not in the immediate sub-epithelial stroma. Duplicate regions of interest were selected for each tissue and segmented based on fluorescence intensity for macrophages, epithelium, and stroma, resulting in 60 segments.

Based on the limit of quantification, 10 segments were removed with a gene detection rate of lower than 10% (Figure 2A). Read counts were normalized for the remaining 50 segments using the quartile 3 (Q3) method. Separation between the geometric mean of the negative control probes, used to calculate the limit of detection, and Q3 of all gene read counts was confirmed at the segment and distribution levels to ensure compatibility with Q3 normalization (Figure 2B). Next, genes detected in less than 10% of segments were removed leaving 7,945 genes (Figure 2C). Overall gene expression across segments was visualized with a Uniform Manifold Approximation and Projection (UMAP) plot, which resulted in two major clusters (Figure 2D). Epithelial segments were contained in one cluster and the second cluster included both stroma and macrophage segments. Notably, segments from the same patient were found in close proximity within each cluster.

Epithelium and Stroma Marker Genes Are Similar in Lesions and Endometrium

We compared the epithelium and stroma segments by tissue type to confirm cell type separation and identify differences in the cell identity in the lesion tissue. The eutopic endometrial epithelium was compared to matching stroma and 1,372 DEG corresponding to cell type were found (Figure 3A). Similarly, there were 1,313 DEG in lesion epithelium versus stroma (Figure 3B) and 14 of the top 20 genes were in common. Gene expression patterns were similar in the endometrium and lesion tissues with a correlation coefficient of 0.81 ($p < 2.2 \times 10^{-16}$, Figure 3C).

103 Stromal and epithelial biological process terms were distinct and consistent with cell type (Figure
104 4D). Vascularization, extracellular matrix, and cell adhesion terms were enriched in the stroma
105 while epithelial cell differentiation and cell-cell junction terms were enriched in the epithelium.
106 Terms were very similar in the stroma with 9 of 10 terms common between the eutopic
107 endometrium and lesions. However, five terms were unique to the lesion epithelium, related to
108 cell-cell adhesion and cell projections or cilia, and two terms to the eutopic endometrial epithelium,
109 cellular transition metal ion homeostasis and circulatory system process.

110 Endometriotic Stroma is Minimally Altered

111 The sub-epithelial stroma from lesions was compared to matched eutopic endometrium to
112 determine transcriptome alterations in endometriotic lesions. Separation of eutopic stroma from
113 the lesions was strongest on PC3, accounting for 12.37% of variation in the dataset (Figure 4A).
114 Two downregulated genes were identified in lesions (Figure 4B), *DHRS1*,
115 dehydrogenase/reductase 1, and *SCGB2A1*, secretoglobin family 2A member 1, both related to
116 steroid metabolism. Six hallmark gene sets [27] were significant in a GSEA, four increased and
117 two decreased (Figure 4C). The increased gene sets were inflammation-related, TNFα signaling
118 via NF-κB, interferon gamma response, interferon alpha response, and inflammatory response,
119 and the decreased gene sets were MYC targets V1 and epithelial mesenchymal transition.

120 Immune Response is Increased in the Endometriotic Lesion Epithelium

121 The endometriotic epithelium was compared to the matched eutopic glandular epithelium
122 and was most separated from the eutopic endometrial epithelium on PC3, representing 9.45% of
123 variation in gene expression (Figure 5A). Differential expression analysis found 76 DEG with 33
124 increased in the lesion epithelium and 43 decreased (Figure 5B). Notably, multiple immune-
125 related genes were increased including, *C3*, or complement 3, *CD74*, *CLU*, or clusterin, and major
126 histocompatibility complex class II members *HLA-DRB1* and *HLA-DPB1*. There were 10
127 significant hallmark gene sets from a GSEA with four terms increased and six decreased (Figure

128 5C). Among the increased gene sets were interferon gamma response and allograft rejection,
129 which matched the increase in immune-related genes in the volcano plot. Genes decreased in
130 response to damage by UV radiation, a source of tissue damage and inflammation, were
131 decreased in lesions. Compared to the eutopic endometrium, glycolysis, angiogenesis, androgen
132 response, and epithelial mesenchymal transition gene sets were decreased in the lesion
133 epithelium. Genes increased in the lesion epithelium were enriched for 33 gene ontology (GO)
134 biological process terms and nine of the top 10 were related to immune response (Figure 5D). In
135 fact, nine of the 33 upregulated genes were associated with positive regulation of immune
136 response: *CD74*, *HLA-DRB1*, *CLU*, *C3*, *HLA-DPB1*, *RPS19*, *HLA-DQB1*, *CFB*, and *VTCN1*.

137 Neither Stroma nor Epithelium Clustered by Tissue

138 Hierarchical clustering dendrograms were plotted for the stromal and epithelial segments
139 (Figures 6A-B) as an unsupervised measure of segment similarity. Neither cell type clustered by
140 eutopic or lesion origin. Segments from two patients were clustered in the stroma and epithelium,
141 that is lesion segments were more like eutopic tissue from the same patient than another lesion.
142 Principal component analyses of the stroma and epithelium (Figures 6C-D) segments revealed
143 that PC1 was driven by patient ID, representing 23.28% and 16.68% of variation in gene
144 expression, respectively.

145 Macrophages are Altered in Peritoneal Lesions

146 Lesion macrophages were most separated from eutopic endometrium macrophages on
147 PC3, representing 8.87% of variation in gene expression (Figure 7A). Differential expression
148 analysis found 148 DEG with 35 increased and 113 decreased in the lesion macrophages (Figure
149 7B). Nine hallmark gene sets were significantly enriched from a GSEA with seven terms increased
150 and two decreased (Figure 7C). The seven increased terms were associated with inflammation
151 and included TNFα signaling via NF-κB, inflammatory response, allograft rejection, and IL2
152 STAT5 signaling. Gene sets that were decreased were myogenesis and epithelial mesenchymal

153 transition. Neither macrophage number nor proximity to the epithelium was altered in lesions
154 compared to eutopic endometrium (Supplemental Figure 1).

155 To provide context for our findings, we sought to compare our results with bulk sequencing
156 data from human peritoneal lesions [21]. Human peritoneal lesions were separated from eutopic
157 endometrium on principal component (PC) one (39.43% of variation) and 3,656 differentially
158 expressed genes (DEG) were identified in an analysis of bulk RNA-sequencing data
159 (Supplemental Figures 2A-C). Gene set enrichment analysis (GSEA) [28] found TNFα signaling
160 via NF-κB, myogenesis, immune response, and adipogenesis hallmark genes [27] increased,
161 while estrogen response, glycolysis, and multiple cell cycle gene sets were decreased in
162 endometriotic lesions (Supplemental Figure 1D).

163 Ligand-Receptor Analysis Identified Epithelium-Macrophage Signaling Axis in 164 Lesions

165 CellChat [29] ligand-receptor analysis was performed to determine the cell-cell
166 communication landscape in endometriotic lesions and eutopic endometrium. Based on 976
167 significant ligand-receptor interactions, 29 signaling pathways were identified in total. Twenty-six
168 pathways were present in lesions, 24 in the endometrium, and 21 pathways were common to
169 both. Three pathways were unique to the endometrium, CXCL, SPP1, and TGF-β, and five unique
170 to lesions, CD45, CD46, ITGB2, PTPRM, and SEMA3. A heatmap of signaling pathways
171 consisting of all possible connections, inter- and intra-tissue, ranked by signaling strength (Figure
172 8A) found collagen signaling to be the strongest followed by MHC-II, laminin, macrophage
173 migration inhibitory factor (MIF) and complement. The three top interacting cell types were lesion
174 stroma, endometrium stroma, and lesion macrophages. Visualization of the cell-cell
175 communication networks in the endometrium and lesions by weight in circle plots showed strong
176 connections from the stroma compartment to the epithelium in both tissue types (Figure 8B).
177 Based on combined network weights, confined to tissue type, the top senders were endometrial

178 (0.172) and lesion stroma (0.170), and the top receivers were lesion macrophages (0.184) and
179 epithelium (0.104). Particularly striking was a 3.70-fold increase in epithelium-to-macrophage
180 signaling in lesions compared to eutopic endometrium. Interaction strength heatmaps (Figure 8C),
181 confirmed the strong connection from the endometrial stroma received by the epithelium. In
182 lesions, the strongest interaction was macrophage-macrophage signaling followed by epithelium-
183 macrophage, surpassing stroma to epithelium signaling. These results point to a strengthened
184 epithelium-macrophage signaling axis in endometriotic lesions.

185 Given that multiple inflammatory pathways were increased in lesions, including MHC-II
186 and complement, and since increased signaling was noted between the lesion epithelium and
187 macrophages, we sought to determine the source of inflammation-related ligands in lesions. A
188 ligand-receptor bubble plot (Figure 9A) demonstrated that complement and MHC-II ligands were
189 originating in the lesion epithelium and likely binding to receptors on macrophages. Within the
190 stroma, MIF was the only visualized inflammatory pathway with likely communication probability
191 indicating that inflammatory signals originated largely in the lesion epithelium. Indeed, a chord
192 diagram of complement signaling (Figure 9B) highlighted the increased complement signaling
193 present in lesions compared to the endometrium and the lesion epithelium as the source.

194 Discussion

195 Endometriosis is a complex reproductive disorder marked by the presence of
196 endometrium-like tissue outside the uterus. Focusing on superficial peritoneal lesions, and
197 excluding deep infiltrating or ovarian endometrioma disease, we hypothesized that endometrium-
198 like tissue in these lesions would display an altered molecular phenotype influenced by the
199 peritoneal microenvironment. To explore this hypothesis, we utilized spatial transcriptomic,
200 receptor-ligand, and bulk RNA-sequencing analyses of endometriotic lesions compared to eutopic
201 endometrium.

202 Bulk RNA-sequencing unveiled thousands of differentially expressed genes (DEGs) and
203 numerous altered inflammatory pathways in lesions compared to the eutopic endometrium,
204 highlighting the inflammatory nature of these lesions and the presence of fibrotic tissue. This
205 observation supported the notion that endometrium-like tissue within the peritoneum would differ
206 significantly from its uterine counterpart. Inflammatory cytokines are increased in the peritoneal
207 fluid of women with endometriosis [30], likely influencing gene expression. Indeed, miRNAs,
208 Notch signaling, aromatase enzymes, prostaglandins, and progestin responsiveness are altered
209 in lesions compared to matched endometrial tissues [31-42].

210 Contrary to our initial expectations, spatial analysis revealed transcriptomic similarities
211 between the three major cell types found in endometrium-like regions of lesions and patient-
212 matched eutopic endometrium, with macrophages displaying the most substantial transcriptional
213 difference. This lack of transcriptional divergence in the epithelium and stroma supports the idea
214 that superficial peritoneal endometriotic lesions are derived from the endometrium following
215 retrograde menstruation [8, 9]. Further, patient rather than tissue type, that is lesion or
216 endometrium, was the primary determinant of gene expression based on principal component
217 and UMAP plots. The differences observed in macrophage gene expression are likely due to the
218 presence of peritoneal and monocyte-derived macrophages in lesions, compared to tissue
219 resident macrophages in the eutopic endometrium [43-45].

220 The discrepancy between bulk RNA-seq and spatial analyses points to the inherent
221 differences in methodologies. While bulk RNA-seq provides a comprehensive view of gene
222 expression changes across the entire homogenized tissue, spatial transcriptomics offers a
223 targeted approach focusing on localized gene expression patterns within distinct regions of
224 interest, such as the endometrium-like structures of lesions. This targeted approach resulted in
225 comparatively few DEG, indicating that the high difference in transcriptomic profiles between
226 lesions and eutopic endometrium found in bulk RNA-seq may not be attributable to endometrium-

227 like tissue in lesions but from the peripheral tissue. This highlights the importance of spatially
228 resolved data in heterogenous tissues like endometriotic lesions. For example, we expect many
229 of the DEG identified in bulk RNA-seq originate from the fibrotic regions of lesions and reflect
230 sustained inflammation and the presence of activated fibroblasts [9, 16]. Interestingly, our findings
231 suggest that the sub-epithelial stroma in superficial peritoneal lesions remains largely unaltered
232 and could serve as an internal control for future spatial experiments, bypassing the requirement
233 for matched eutopic stromal tissue. The paired design of this study increased power with a limited
234 sample size. However, the lack of healthy control endometrium and unknown time since symptom
235 onset are notable caveats and may limit the generalizability of the findings, particularly for the
236 initiation of disease. As such, further research is necessary to elucidate the molecular
237 mechanisms underlying the early pathogenesis of superficial peritoneal endometriosis.

238 The spatial transcriptomic technique, sequencing hybridized probes from specific areas of
239 FFPE tissue, resulted in an overall reduced transcriptome size after removing genes with low
240 counts across segments. The spatial transcriptome included 7,945 genes while the bulk RNA-
241 sequencing analysis included 17,405 genes. Consequently, many of the lowest expression genes
242 from the bulk RNA-sequencing data were filtered from the spatial transcriptome before DEG
243 analysis. The advantage of spatial transcriptomics, however, is gaining information from genes
244 expressed only by a subset of cells or a single cell type that would be lost in the bulk tissue. This
245 is evidenced by the inclusion of 551 genes in the spatial transcriptome that were considered as
246 not expressed in the bulk RNA-sequencing analysis. Further, spatial transcriptomics indicated
247 increased proliferation of the lesion epithelium while bulk RNA-sequencing found an overall
248 reduction in cell cycle gene sets. The epithelium of lesions is likely to be a minor contributor to
249 gene expression from homogenized tissue since lesions often have little or even no remaining
250 epithelial component. Interestingly, these results suggest the lesion epithelium may proliferate in
251 response to inflammatory peritoneal environment while stroma reduces proliferation and may

252 even become senescent [46] . A growing body of evidence has found that senescence plays a
253 role in multiple pathologies and may contribute to endometriotic lesions [47-49].

254 Receptor-ligand analysis identified an almost four-fold increase in signaling between
255 epithelium and macrophages in lesions compared to the endometrium, including multiple
256 inflammatory pathways. MHC-II ligands expressed in the lesion epithelium were predicted to
257 communicate to macrophages through the CD4 receptor. Notably, human monocytes and
258 macrophages express CD4, unlike the mouse, serving as an important target for HIV-1 infection
259 [50-52]. The canonical macrophage marker from this study, CD68, is expressed by monocytes
260 and macrophages [53]. Although monocytes rapidly differentiate into macrophages within a tissue,
261 some monocytes were likely included in the spatial transcriptome analysis. Canonically, MHC-II
262 binding of the CD4 receptor on monocytes promotes differentiation into macrophages [51], thus
263 increased MHC-II in the lesion epithelium would drive macrophage differentiation from circulating
264 monocytes homing to areas of hypoxia and inflammation. Increased expression of MHC class II
265 expression in the epithelium aligns with recent single cell RNA-sequencing analysis of ovarian
266 endometriosis, which found increased MHC class II expression in the epithelium [54].

267 Macrophage migration inhibitory factor (MIF) is constitutively expressed by many cell
268 types and has pleiotropic autocrine and paracrine proinflammatory effects on tissues [55]. MIF
269 signaling in macrophages sustains proinflammatory function by inhibiting apoptosis,
270 counteracting the immunosuppressive effects of glucocorticoids, and promoting secretion of
271 prostaglandin E2 [55, 56]. Additionally, MIF is released by monocytes, macrophages, and other
272 immune cells upon exposure to proinflammatory mediators, such as C3, to reinforce a local
273 proinflammatory environment [57-59].

274 *Complement 3* expression was increased in bulk RNA-sequencing results (3.7-fold, FDR
275 $p = 0.0003$) and found in the lesion epithelium from spatial transcriptomic analysis (4.6-fold, FDR
276 $p = 0.003$). Endometriotic lesions were originally reported to express Complement 3 (C3) by

277 Weed and Arquembourg in 1980 [60] and later found to be secreted by the lesion epithelium [61,
278 62]. In fact, serum levels of C3 are elevated in patients with endometriosis and C3 was proposed
279 as a potential diagnostic biomarker [63]. The complement system is a signaling cascade that plays
280 a pleiotropic role in immune response, including production of proinflammatory mediators and
281 recognition and clearance of pathogens by lysis and enhanced phagocytic uptake by immune
282 cells [64]. The cascade of over 50 proteins is characterized by a series of protein cleavage events
283 that produce inflammatory cytokines and the components for subsequent steps. Multiple stimuli
284 can activate the complement system, but all pathways converge on activation of C3 by a
285 convertase. Although the presence of C3 in endometriotic lesions has been known for 40 years,
286 its potential contribution to the disease is unclear [65]. Following cleavage, the resulting fragments
287 are referred to by appending the letter “a”, for the smaller fragment, or “b”, for the larger fragment,
288 to the protein name, for example, C3a.

289 C3a and C3b are produced following activation of C3 by a C3 convertase, itself the product
290 of prior cleavage events. C3b induces phagocytic activity of macrophages, but lesion tissue is
291 refractory to complement targeting through multiple mechanisms. CD47, otherwise known as the
292 “don’t eat me signal”, is expressed by tissue and binds to the SIRPα receptor on macrophages,
293 inhibiting phagocytosis [66, 67]. Complement regulatory proteins, such as CD35, CD46, and
294 CD55, inhibit complement attack by accelerating breakdown or direct cleavage of complement
295 components critical for continuation of the cascade [64]. In the event of complement activation,
296 CD59, another complement regulatory protein, inhibits formation of the membrane attack complex
297 and prevents cell lysis [68]. Thus, multiple mechanisms exist within the lesion to prevent direct
298 complement attack but complement signaling promotes a localized proinflammatory environment.

299 The proinflammatory cytokine C3a, released following C3 cleavage, can activate a pro-
300 repair or tumor-associated macrophage (TAM) phenotype by binding to C3AR1, as found in the
301 ligand-receptor analysis [69]. This provides a mechanism by which C3 activation from the

302 superficial peritoneal endometriotic lesion epithelium promotes the pro-lesion macrophage
303 phenotype described as pro-repair, tumor-associated, or M2. These macrophages then contribute
304 to lesion tissue remodeling including neovascularization and fibrosis [18, 70, 71]. Additionally,
305 semaphorin 3B was found in the lesion epithelium signaling to macrophages and could further
306 promote the pro-disease TAM phenotype since SEMA3B increased expression of pro-repair
307 macrophage markers in a model of rheumatoid arthritis [72].

308 Activated complement signaling in tissue induces a diffuse inflammatory state that
309 includes increased prostaglandins, also upregulated by MIF [65]. Increased prostaglandins can
310 activate steroidogenic enzymes and, potentially the production of estradiol and estrone by the
311 lesion [31, 33, 35, 73]. Finally, increased estrogens can activate complement in lesion tissue [74]
312 resulting a positive feedback loop, common in pathogenic signaling. In this manner, the
313 complement signaling is sustained by local estrogenic activity and could sustain local
314 inflammation and the presence of pro-repair macrophages until such time as the lesion becomes
315 completely fibrotic with a tissue stiffness that no longer supports cell growth and the lesion
316 becomes scar tissue and contributes to peritoneal adhesions. In support of complement signaling
317 promoting lesion pathogenesis, C3 null uterine tissue formed fewer lesions after 21 days in a
318 mouse model of endometriosis [75].

319 The comparison of lesions to eutopic endometrium yielded intriguing insights into the
320 molecular and cellular dynamics underlying lesion pathophysiology. Firstly, despite previous
321 findings from bulk tissue analysis suggesting significant differences between endometrium-like
322 tissue in lesions and eutopic endometrium, our spatial transcriptomic data reveal a surprising
323 similarity between these two tissues. The lack of drastic differences may be attributed to the
324 composition of the excised lesions used in bulk RNA-sequencing, with endometrium-like tissue
325 comprising only a small proportion of the lesion, such that differential expression was largely
326 attributable to the peripheral stroma and fibrotic tissue. Notably, this difference highlights the

327 importance of employing advanced techniques, like spatial transcriptomics, to gain an improved
328 understanding of lesion biology.

329 Secondly, spatial transcriptomics has provided novel insights into the intricate cellular
330 crosstalk within lesions. Our data indicate signaling between the stroma and epithelium, as well
331 as between the lesion epithelium and macrophages. Notably, the epithelium emerged as a central
332 player in driving inflammation within the lesion, promoting inflammatory signaling independent of
333 the stromal compartment. Moreover, the presence of CD68+ cells amid epithelial cells highlights
334 the physiological relevance of cell-cell interactions across different cell types.

335 Drawing from these observations, we present a model wherein the superficial lesion
336 epithelium orchestrates inflammatory signaling within the lesion while promoting a pro-repair
337 phenotype in infiltrating macrophages. Spatial transcriptomics facilitated the identification of
338 inflammatory signaling emanating from the epithelium, including C3, MIF, and MHC class II. This
339 novel insight sheds light on the pathological consequence of C3 expressed by the epithelium in
340 modulating macrophage phenotype to support lesion development. In summary, our study
341 underscores the critical role of considering spatial context and cellular interactions within lesions
342 to unravel the complexities of superficial peritoneal endometriotic lesions. Further investigation is
343 imperative to elucidate the specific mechanisms governing epithelium-driven inflammation and its
344 implications for disease progression and therapeutic intervention.

345

346 Methods

347 Human Tissues

348 All protocols involving tissue collection were approved by the institutional review board
349 (IRB) Committee of Ponce Health Sciences University, School of Medicine (PHSU). Endometriotic
350 lesions and matched eutopic uterine tissues from 10 patients were obtained as archived
351 deidentified formalin-fixed paraffin-embedded (FFPE) tissue blocks [76-78]. All tissues were

352 previously evaluated by a pathologist to confirm the diagnosis of endometriosis and menstrual
353 cycle stage of eutopic endometrium using Noyes criteria [79].

354 Histology

355 Tissue blocks were sectioned and trichrome stained (StatLab #KTTRBPT) to confirm the
356 presence of defined epithelial and stromal compartments in lesions. Blocks were serial sectioned
357 at 6 μm thickness and floated onto positively charged microscope slides. Tissues were attached
358 to the slides prior to processing by heating on a slide warmer for 15 minutes. Tissues were then
359 deparaffinized and rehydrated through three changes each of xylenes for five minutes and 100%
360 ethanol for one minute before a rinsing in running tap water for one minute. Slides were incubated
361 in Bouin's fluid at room temperature overnight. Slides were rinsed in running tap water for three
362 minutes and immersed in modified Mayer's hematoxylin stain for four minutes at room
363 temperature. After a three-minute rinse in running tap water, slides were immersed in one step
364 trichrome stain for five minutes and rinsed in running tap water for five seconds. Slides were then
365 dehydrated through three changes of 100% ethanol for one minute, cleared in three changes of
366 xylenes for one minute, and a coverslip was applied with Permount mounting medium (Fisher
367 Scientific #SP15).

368 Spatial Transcriptomics

369 Human tissue slide preparation, library generation, and sequencing for digital spatial
370 profiling (DSP) on the NanoString GeoMx DSP instrument were performed by the Van Andel
371 Institute Histology and Genomics Cores. Sections were cut at 5 μm thickness and mounted on
372 plus-charged slides (Epredia Colormark Plus #CM-4951WPLUS-001). Slides were baked at 60°C
373 for one hour and stored at 4°C in a vacuum-sealed container containing desiccant for up to two
374 weeks. All subsequent steps were performed under RNase-free conditions with DEPC-treated
375 water. Slides were deparaffinized with three sequential five-minute washes in xylenes, followed
376 by two washes in 100% ethanol for five minutes, one wash in 95% ethanol, and one wash in 1X

377 PBS. Antigen retrieval was performed in target retrieval reagent (EDTA, pH 9.0; Invitrogen #00-
378 4956-58) diluted to 1X in the BioGenex EZ-Retriever System for 10 minutes at 95°C. Slides were
379 then washed with 1X PBS for five minutes. Slides were then incubated in 1 µg/mL proteinase K
380 10 minutes at 37°C and washed in 1X PBS for five minutes at room temperature. Slides were
381 fixed for five minutes in 10% neutral buffered formalin followed by two washes in NBF stop buffer,
382 for five minutes each, and one wash in 1X PBS for five minutes. Slides were then incubated with
383 UV-photocleavable Human Whole Transcriptome Atlas hybridization probes diluted in buffer R
384 (GeoMx RNA Slide Prep FFPE-PCLN kit, #121300313) in a hybridization oven at 37°C for 16-20
385 hours. Following probe incubation, slides were washed with stringent buffer (1:1, formamide:4X
386 SSC buffer; Thermo Fisher #AM9342; Sigma-Aldrich #S6639) at 37°C twice for 25 minutes each.
387 Then slides were washed twice in 2X SSC buffer. Slides were blocked in 200 µL buffer W (GeoMx
388 RNA Slide Prep FFPE-PCLN kit) for 30 minutes and incubated at 4ºC overnight with SYTO 13
389 nucleic acid stain (500 nM; Thermo Fisher Scientific #S7575) and antibodies for pan-cytokeratin
390 (panCK; 1 µg/mL; Novus Biologicals #NBP2-33200AF488), smooth muscle actin (ACTA2; 1.25
391 µg/mL; Abcam #ab202368), and CD68 (0.5 µg/mL; Santa Cruz Biotechnology #sc-20060AF647)
392 diluted in buffer W. Slides were washed four times in 2X SSC buffer for 3 minutes each and placed
393 in the NanoString GeoMx DSP instrument.

394 Duplicate 500 μm^2 regions of interest (ROI) were selected for each based on fluorescent
395 imaging on the GeoMx DSP instrument (NanoString Technologies). ROI were drawn in the central
396 portion of the endometrium stratum functionalis, to include glandular and not luminal epithelium,
397 for eutopic uterine tissue and in lesions areas with defined epithelium. ROIs were then segmented
398 in order of macrophages (CD68+), epithelium (panCK+), and stroma (ACTA2-) areas of
399 illumination (AOI) for individual collection. AOI were processed sequentially on the instrument
400 using UV light focused through each AOI that released the photocleavable oligos into wells of a
401 96 well plate. After AOI collection, indexing primers were hybridized during NanoString library

402 preparation. Quality and quantity of the finished library pools were assessed using a combination
403 of Agilent DNA High Sensitivity chips (Agilent Technologies, Inc.) and the QuantiFluor dsDNA
404 System (Promega Corp.). Paired-end, 50 bp sequencing was performed on an Illumina Novaseq
405 6000 sequencer using an S2, 100 cycle sequencing kit v1.5 (Illumina Inc.). Base calling was done
406 by Illumina RTA3 and output was demultiplexed and converted to fastq format with bcl2fastq
407 v1.9.0.

408 ## Spatial Data Analysis

409 Fastq files were converted to digital count conversion (DCC) files using GeoMx NGS
410 Pipeline v2.3.3.10. Sample annotation, PKC configuration, and DCC files were imported with
411 GeomxTools (v3.2.0) in R to generate a NanoStringGeoMxSet object. Read counts with a value
412 of zero were shifted to one for downstream transformations and quality control (QC) analyses.
413 Each AOI, or segment, was assessed for sequencing and tissue quality using the parameters
414 listed in **Box 1**. Outlier probes were then excluded before counts were collapsed to gene-level
415 data (18,677 genes) by geometric mean. The limit of quantification (LOQ) was determined per
416 segment based on the distribution of negative control probes and set at two geometric standard
417 deviations above the geometric mean with a minimum value of two. Segments with a gene
418 detection rate less than 10% were filtered before removing genes detected in less than 10% of
419 segments. Separation between the upper quartile 3 (Q3) of gene counts and the geometric mean
420 of the negative probes was confirmed before count normalization using the quartile 3 (Q3)
421 method.

422 Normalized read counts were $\log_2$-transformed and dimension reduction was performed
423 by uniform manifold approximation and projection (UMAP) [80] with the umap package (v0.2.10)
424 with the random state set to 42. Differential expression analyses were completed using $\log_2$-
425 transformed normalized read counts with a linear model approach in the limma package (v3.54.2)
426 [81]. A linear model was fit for each gene with lmFit before an empirical Bayes test was completed

427 using patient as a covariate. P-values were corrected for multiple testing with the Benjamini
428 Hochberg method included in the decideTests function of limma. Genes were considered
429 differentially expressed when the adjusted p-value was below 0.05. Principal component analysis,
430 volcano plots, gene set enrichment analysis, and over-representation tests were completed as
431 described for bulk RNA-sequencing data.

432 Macrophage Quantification

433 The macrophage count distance between from epithelium was manually measured for
434 each segment using the line tool in ImageJ software [82]. The global scale was set by measuring
435 the scale bar on the image (1 pixel = 2.51 μm). For each image, the green epithelium and red
436 macrophage channels were merged for analysis. A line was drawn from the center of each
437 macrophage to the center of the closest epithelial cell and the measurements. Based on these
438 measurements the macrophages count and the average distance for each segment was
439 calculated. Data were analyzed in Prism (v10.2.2, GraphPad Software LLC) following
440 confirmation of normality (Shapiro-Wilk, $p > 0.1$). To determine if there was a relative increase in
441 lesions compared to the matched endometrium, macrophage count was tested using a ratio
442 paired t-test. Macrophage distance to the nearest epithelium was tested using a paired t-test.

443 Bulk RNA-sequencing Analysis

444 Read counts per gene were downloaded from eutopic endometrium (n = 7) and peritoneal
445 endometriotic lesion samples (n = 6) for series GSE179640 [21] from the NCBI Gene Expression
446 Omnibus repository. Files were parsed with R (version 4.2.0) and all subsequent analyses, unless
447 otherwise noted, were completed in R using RStudio [83]. Differential expression analysis was
448 conducted using the edgeR-robust method (v4.0.3) [84, 85]. Genes with low counts per million
449 (CPM) were removed using the filterByExpr function from edgeR. Multidimensional scaling plots,
450 generated with the plotMDS function of edgeR, were used to investigate group separation prior
451 to statistical analysis. Principal component analysis of normalized $\log_2$-transformed CPM was

conducted with the PCAtools package (v2.10). The biplot and pairsplot functions were used to visualize sample separation across principal components one through five. Differentially expressed genes (DEG) were identified based on Benjamini-Hochberg false discovery rate (FDR) p-values less than 0.05. The hclust function was used for hierarchical clustering (ward.D2) of Euclidean distances and plotted with the dendextend package (v1.17.1). A volcano plot was generated with EnhancedVolcano (v1.16) and the top 20 DEG, based on FDR p-value, were labeled. Gene set enrichment and over-representation analyses were completed with clusterProfiler package (version 4.6.0) [86] using mSigDB [27] reference databases.

Receptor-Ligand Analysis

Quantile-normalized read counts were used for receptor-ligand analysis with the CellChat package (1.6.10) in R [29]. Significant genes and interactions were identified using the functions `identifyOverExpressedGenes` and `identifyOverExpressedInteractions`. Communication probabilities were calculated between cell types with raw input counts option enabled, as recommended for bulk-sequencing data. The resulting interactions were visualized using the included plotting functions. Weighted communication probabilities were subset for eutopic endometrium or lesions before calculating tissue-specific communication interaction strengths.

Data Availability

Sequence data from the spatial transcriptomics experiment were deposited in the NCBI Gene Expression Omnibus and available under series GSE263897.

Acknowledgements

The authors would like to sincerely thanks all members of the Fazleabas laboratory and the Van Andel Genomics core, particularly Becca Siwicki, for their contributions to this project. This work was supported by NanoString Technologies, Incorporated (GWB) and National Institutes of Health grants F32HD104478 (GWB), R01HD099090 (ATF), R01HD050559 (IF),

U56CA126379 (IF), and T32HD087166 (GWB, ATF). The content is solely the responsibility of the authors and does not necessarily represent the official views of the National Institutes of Health.

Author contributions

Conceptualization, G.W.B., E.G., and A.T.F.; Data curation, G.W.B, Z.F., Z.B.M, and I.F.; Formal analysis, G.W.B, Z.F., E.L.V, and Z.B.M.; Funding acquisition, G.W.B, I.F, and A.T.F.; Investigation, G.W.B and E.L.V.; Methodology, G.W.B, Z.F., E.L.V, and Z.B.M; Resources, I.F. and A.T.F; Software, G.W.B, Z.F., and Z.B.M; Supervision, E.G. and A.T.F; Visualization, G.W.B; Writing – original draft, G.W.B and A.T.F.; Writing – review & editing, G.W.B, Z.F., E.G., I.F., and A.T.F.

Declaration of interests

The authors declare no competing interests.

Declaration of generative AI and AI-assisted technologies in the writing process

During the preparation of this work, the authors used ChatGPT (v3.5) for proofreading and to improve readability. After using this service, the authors reviewed and edited the content as needed and take full responsibility for the content of the publication.

494 # Figures

Figure 1

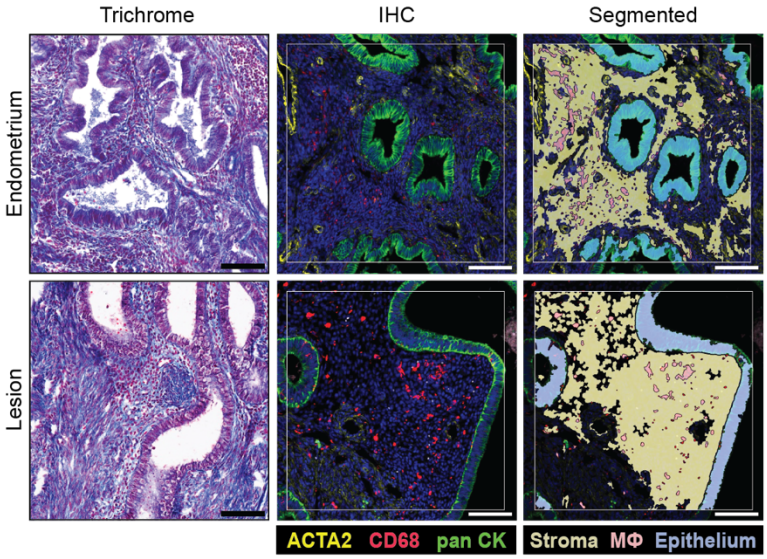

495 ## Figure 1

496 Segmentation strategy for spatial transcriptomics. Superficial peritoneal endometriotic lesions and
497 matched endometrium (n = 10) were visualized with trichrome staining to confirm the presence of
498 epithelial and stromal compartments. Tissues were immunostained for pan-cytokeratin, CD68,
499 and ACTA2 for segmentation and spatial transcriptome collection on the GeoMx platform.
500 Representative regions of interest (ROI) are shown for each tissue type. Duplicate ROI were
501 collected for each tissue and stroma, epithelium, and macrophages were segmented from each
502 for a total of 20 ROI and 60 segments. Scale bar = 100 μm.

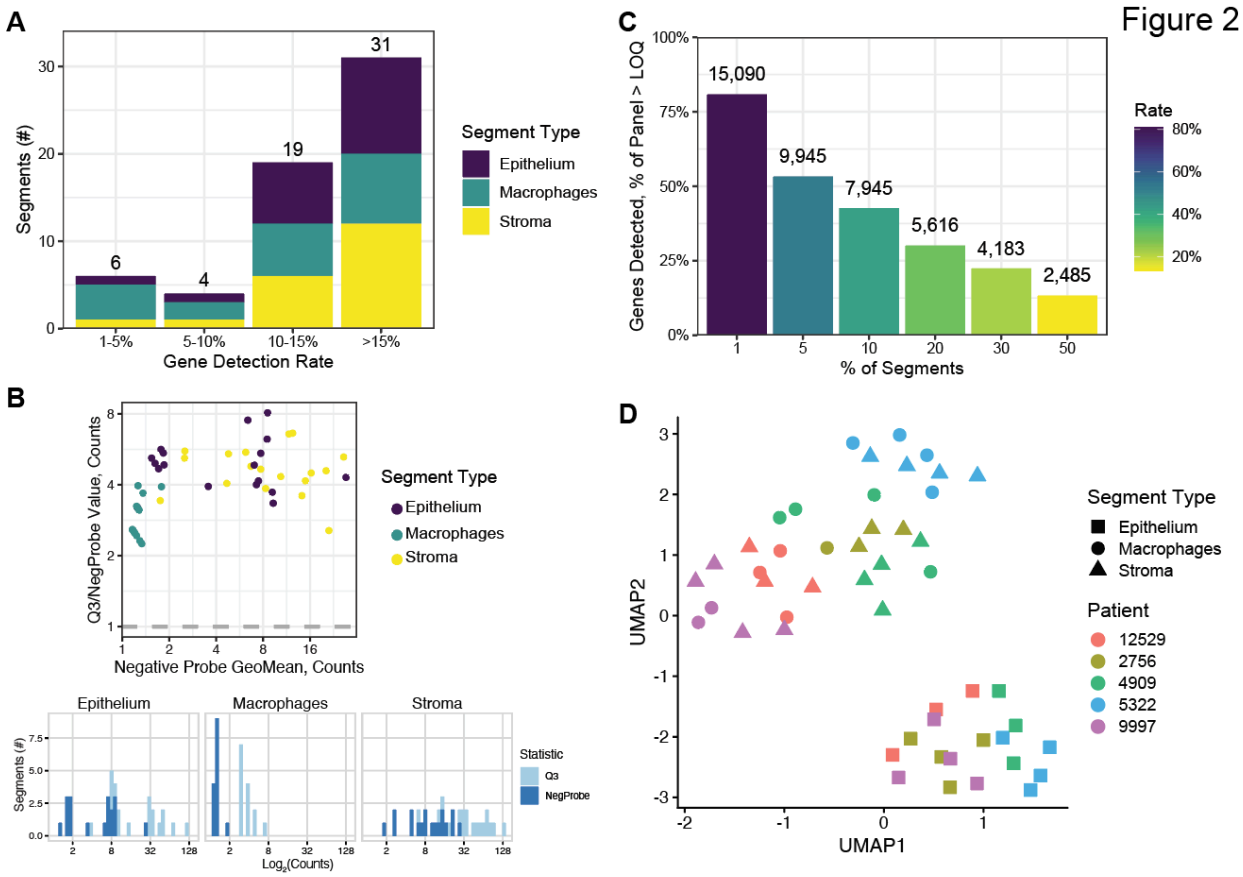

Figure 2

Spatial transcriptomics results from eutopic endometrium superficial peritoneal endometriotic lesions. (A) Bar plot of all 60 segments separated by gene detection rate. Segments with a detection rate of less than 10% were removed. (B) Confirmation of gene and negative probe count separation by segment in a scatter plot and by distribution for each cell type in histograms. Separation after gene and segment filtering is required for effective Q3 normalization. (C) Bar plot of detectable genes per segment used for filtering genes found in less than 10% of segments leaving 7,945 genes for further analysis. (D) Dimensionality reduction UMAP plot of all segments coded by shape and colored by patient. Epithelium clustered separately from stroma and macrophages.

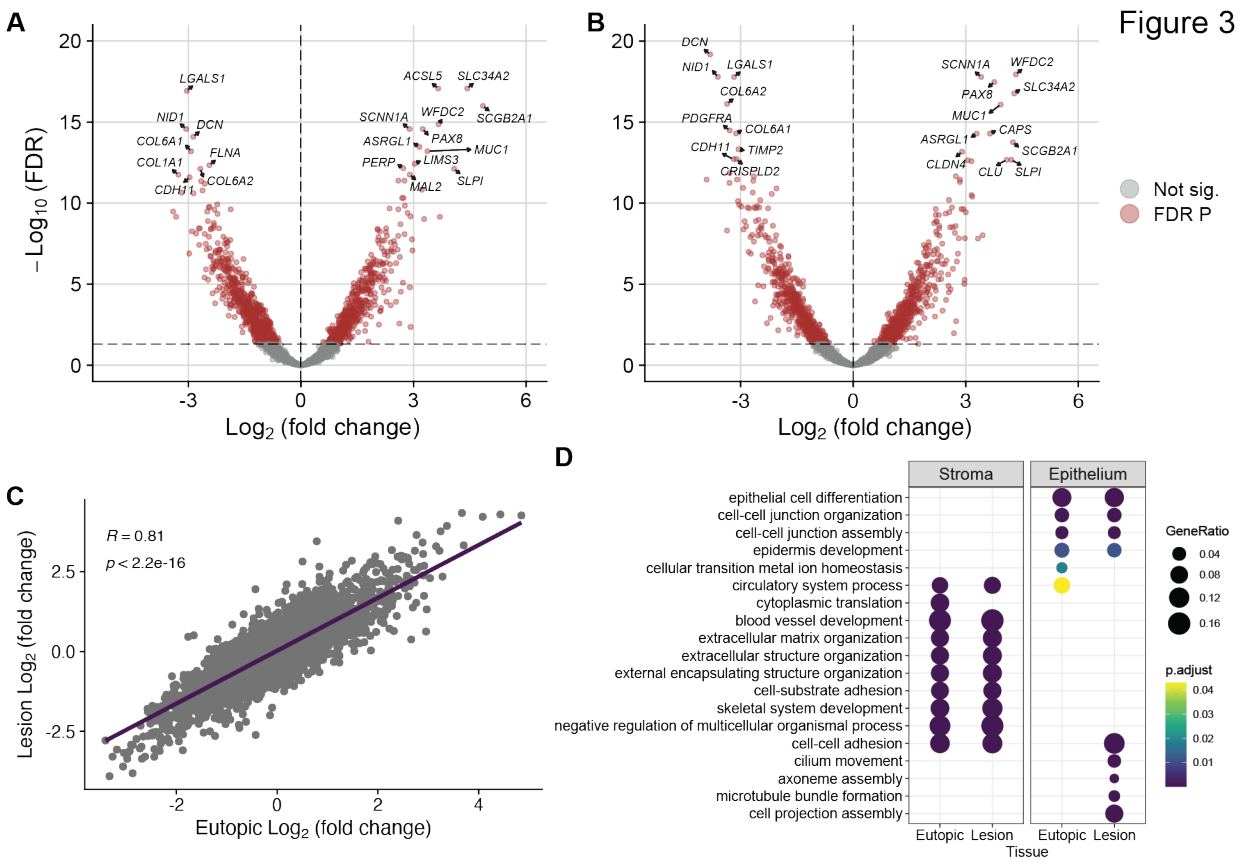

Figure 3

Epithelium versus stroma in eutopic endometrium and lesions. Volcano plots of differentially expressed genes (DEG) in the (A) endometrium and (B) lesions. The top DEG were similar in volcano plots with canonical epithelial genes like *MUC1*, *PAX8*, and *WFDC2* increased in both epithelia. (C) Genes enriched for each compartment were highly correlated in the eutopic endometrium and lesions. (D) Enriched gene ontology biological process terms were consistent with cell type, including extracellular matrix genes in the stroma and cell-cell junction genes in the epithelium, in the eutopic endometrium and lesions. Several terms related to cell-projections and cilia were unique, however, to the lesion epithelium.

Figure 4

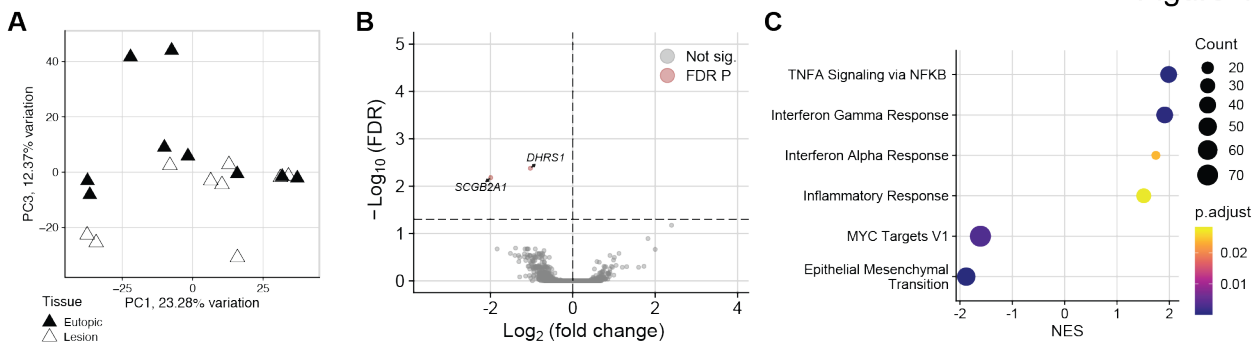

Figure 4

Endometriotic sub-epithelial stroma is minimally altered compared to eutopic endometrium. (A) Principal component (PC) plot of lesion stroma compared to eutopic endometrium showed group separation most clearly on PC3. (B) Volcano plot of two down-regulated genes in the endometriotic stroma. (C) Gene set enrichment analysis of hallmark pathways found four increased inflammatory gene sets and two decreased.

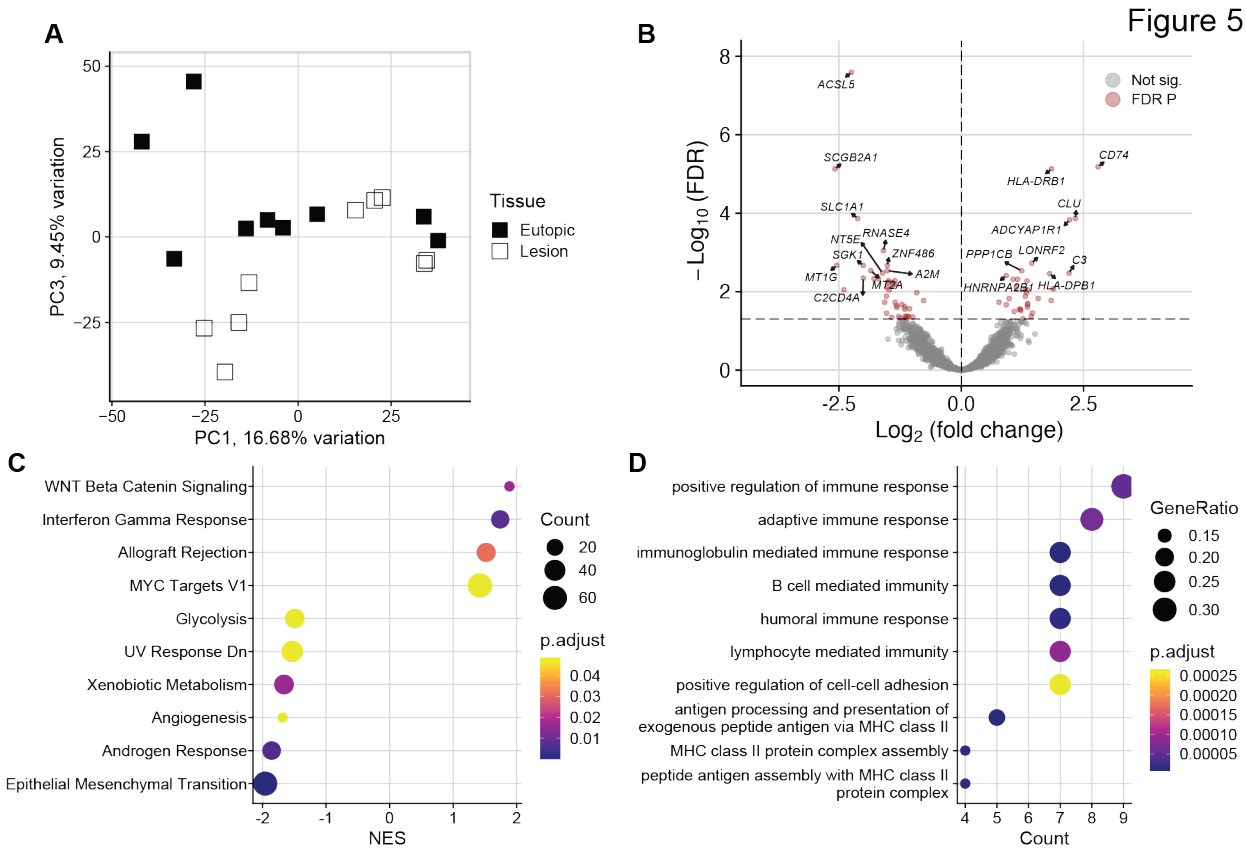

Figure 5

Immune response genes are increased in the endometriotic lesion epithelium. (A) Principal component (PC) plot of lesion epithelium compared to eutopic endometrium showed group separation most clearly on PC3. (B) Volcano plot of 76 differentially expressed genes (DEG) in the endometriotic epithelium. Of note, complement 3, *C3*, was one of the top increased DEG and several others were major histocompatibility complex class II related genes, like *CD74* and *HLA-DRB1*. (C) Gene set enrichment analysis of hallmark pathways found four increased gene sets and six decreased, indicating increased inflammation and proliferation. (D) Nine of the top 10 enriched gene ontology biological process terms were immune related.

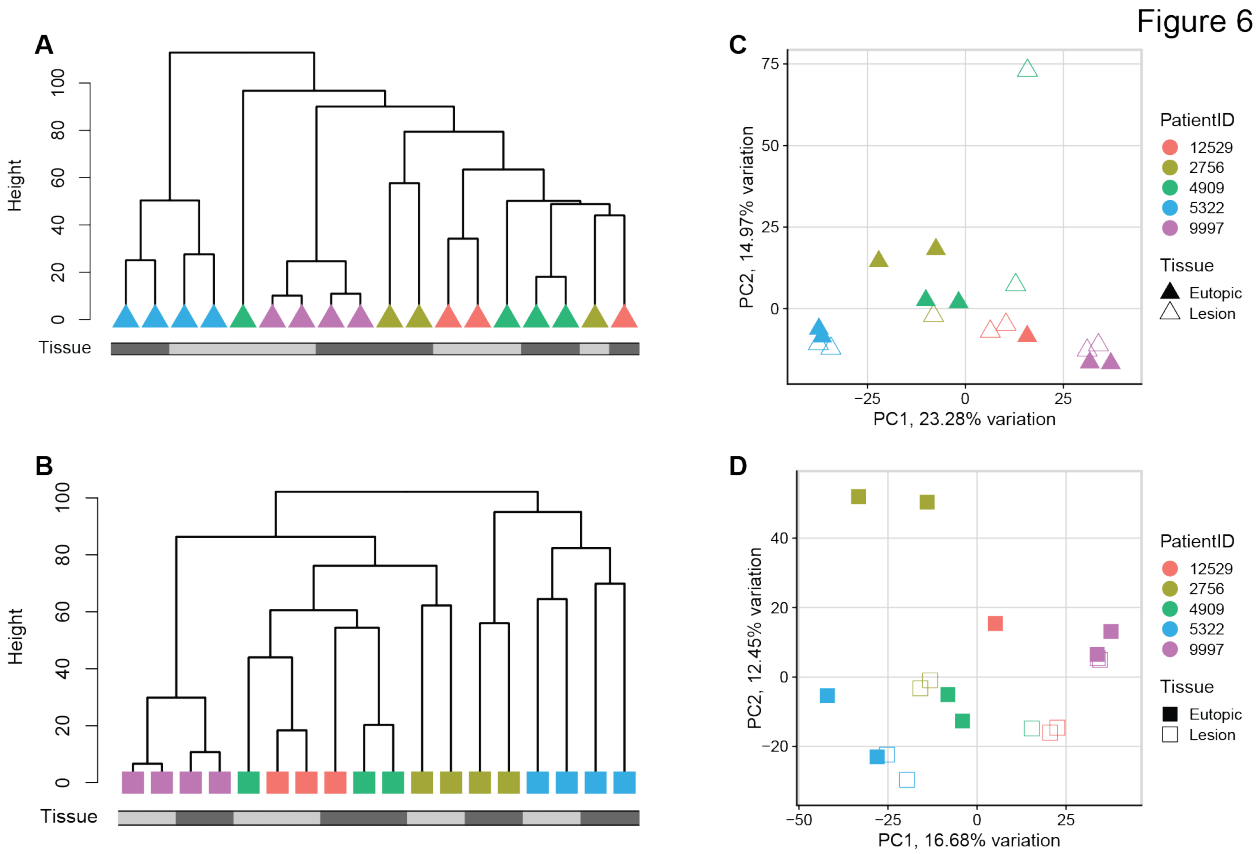

Figure 6

Neither stroma nor epithelium cluster by lesion versus eutopic endometrium. Hierarchical clustering dendrograms of (A) stroma and (B) epithelium segments found no clustering of segments by tissue of origin (endometrium = black bar). Principal component (PC) plots demonstrated that PC1, the largest component of variation, was correlated with patient identity.

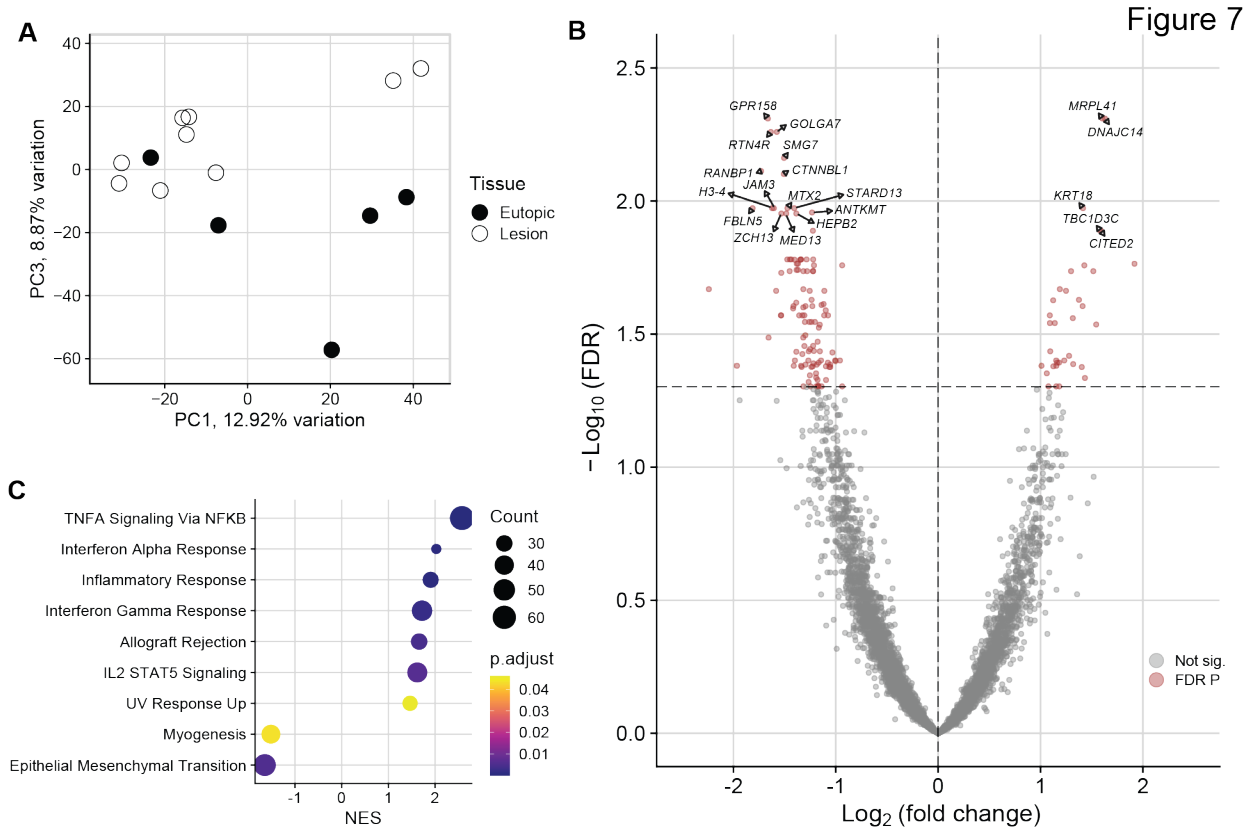

Figure 7

Macrophages are altered in endometriotic lesions. A) Principal component (PC) plot of lesion macrophages compared to eutopic endometrium showed group separation most clearly on PC3. (B) Volcano plot of 148 differentially expressed genes (DEG) in the endometriotic macrophages. (C) Gene set enrichment analysis of hallmark pathways found seven increased gene sets and two decreased, indicating increased inflammation likely reflective of the presence of monocyte-derived macrophages in the lesion tissue.

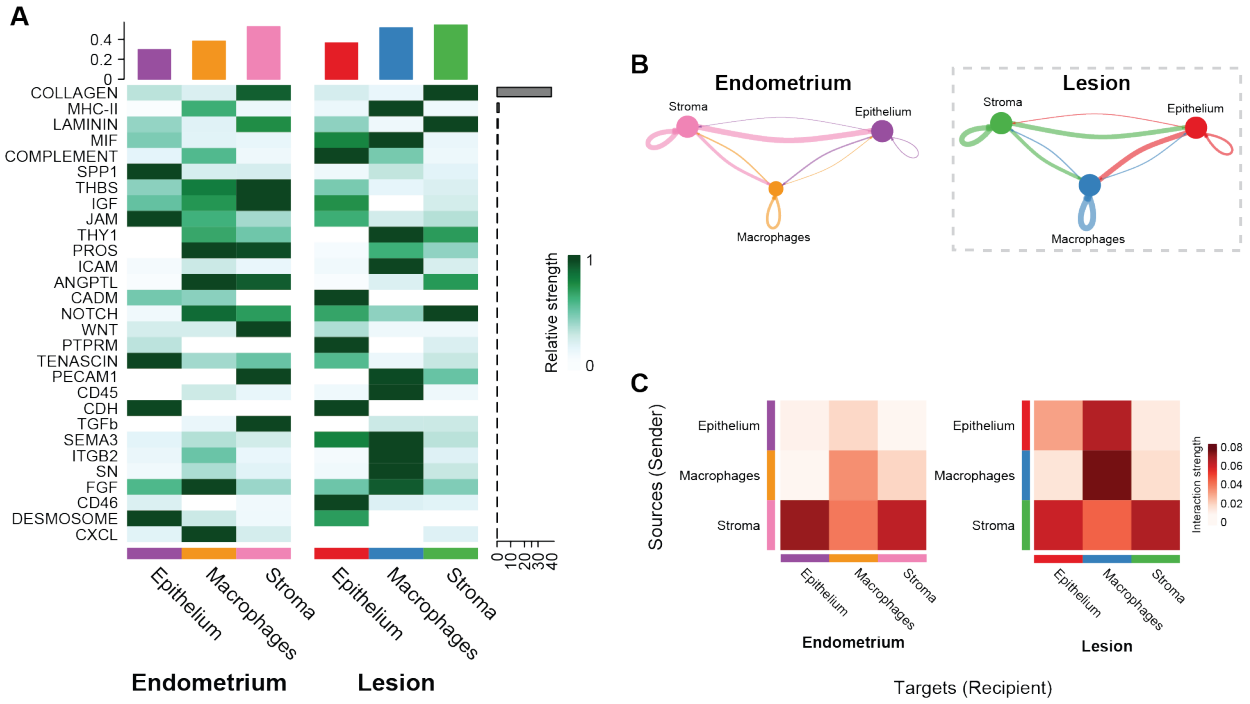

Figure 8

CellChat ligand-receptor analysis identified increased communication from the lesion epithelium to macrophages. (A) Signaling pathway heatmap of all 29 significant pathways identified by CellChat sorted by signaling strength, indicated by the gray bar. Interactions, combined incoming and outgoing, totaled for each cell type in the bar plot at the top of the heatmap and scaled per row. (B) Circle plots of communication networks including 24 pathways in the endometrium and 26 in lesions where line thickness corresponds to strength. Stroma to epithelium communication was strong in the eutopic endometrium and similarly present in the lesions. However, epithelium to macrophage communication was increased 3.7-fold in lesions. (C) Interaction strength heatmaps highlight the gain of epithelium to macrophage signals in lesions and strong macrophage-macrophage interactions.

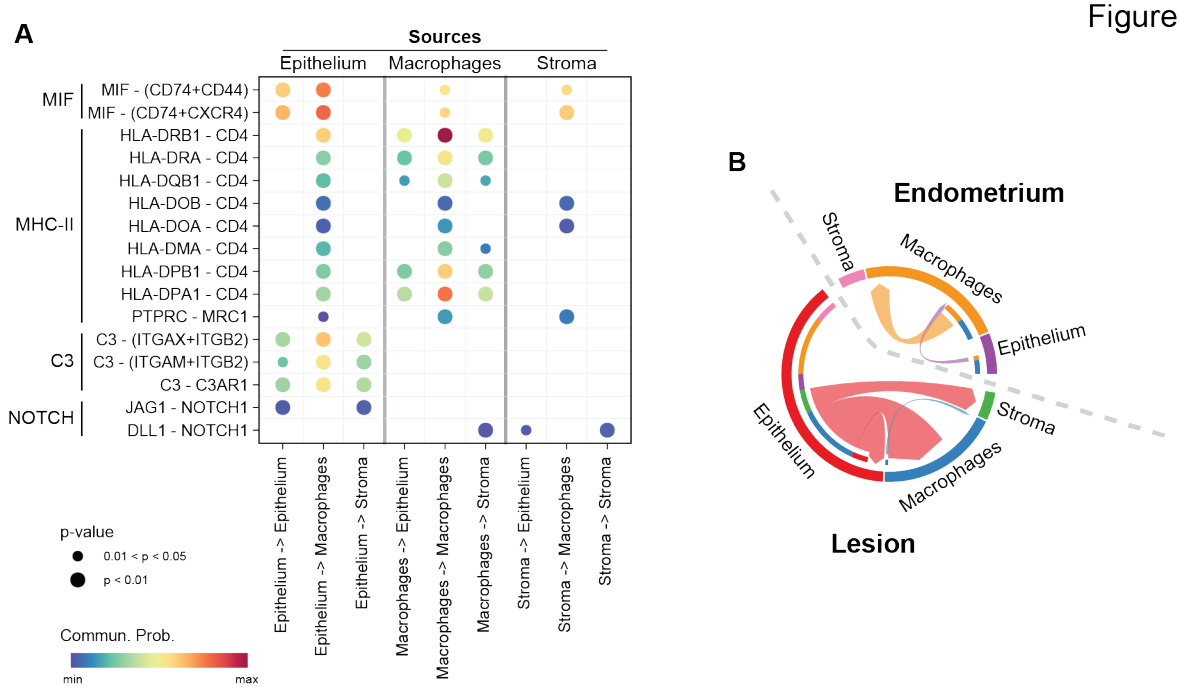

Figure 9

Inflammatory ligands originate in the endometriotic lesion epithelium. (A) Ligand – receptor dot plot of inflammatory pathways in endometriotic lesions. Pathway names are indicated on the left side of the plot followed by specific ligand and receptor interactions. All signals originating from the lesion epithelium are in the left three columns, macrophages in the center, and stroma on the right. Complement and major histocompatibility complex class II (MHC-II) pathways originated in the lesion epithelium and not the stroma. Macrophage migration inhibitory factor (MIF) signaling was strongest in the epithelium, but also sent from the stroma and macrophage cell types. (B) Complement signaling chord diagram of the weighted complement signaling pathway indicating increased signaling from the lesion epithelium compared to the eutopic endometrium epithelium.

```
minSegmentReads = 1000,
percentTrimmed = 80,
percentStitched = 80,
percentAligned = 75,
percentSaturation = 40,
minNegativeCount = 1,
maxNTCCount = 9000,
minNuclei = 20,
minArea = 1000
```

573 ## Box 1

574 Spatial transcriptomics quality control parameters for segment filtering.

575

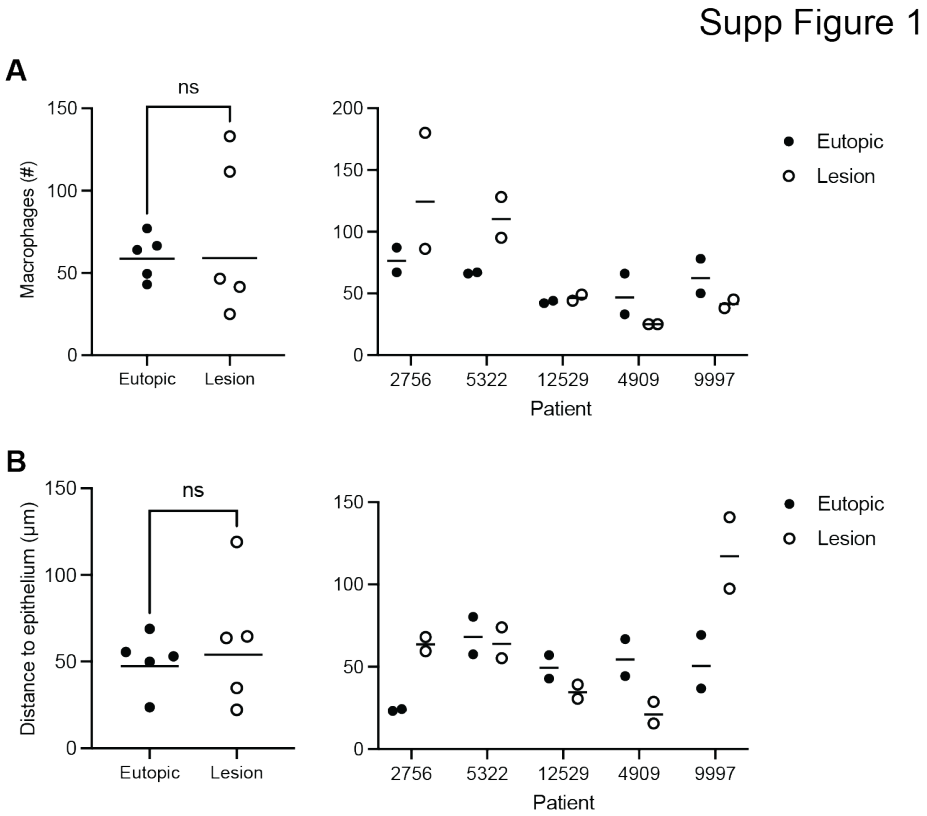

576 ## Supplemental Figure 1

577 Quantification of macrophages in spatial transcriptomic segments from eutopic endometrium and
578 superficial peritoneal lesions. Data are shown by group and individual patient. (A) Macrophage
579 number was not increased in lesions ($p = 0.98$) and (B) did not appear to be located closer to the
580 lesion epithelium ($p = 0.59$).

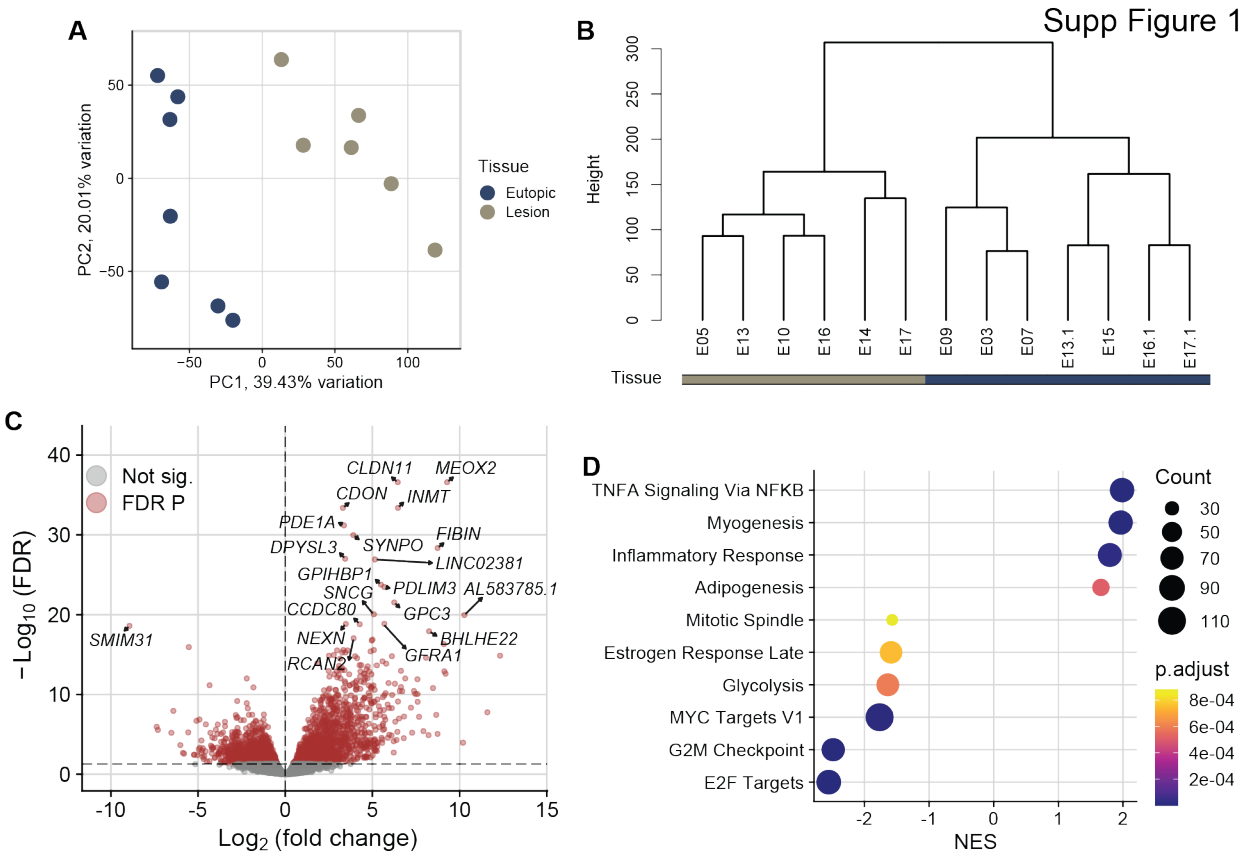

Supplemental Figure 2

Transcriptome alterations in superficial endometriotic lesions compared to eutopic endometrium as measured by bulk RNA-sequencing. (A) Principal component (PC) plot of superficial peritoneal endometriotic lesions and eutopic endometrium (n = 13) from GSE179640. Samples were separated across PC1 by tissue type, representing 39% of variation in gene expression. (B) Hierarchical clustering dendrogram confirmed separation of lesions from eutopic endometrium. (C) Volcano plot of 3,656 differentially expressed genes in lesions versus endometrium. (D) Gene set enrichment analysis of hallmark pathways found inflammation, represented by TNFα signaling via NF-κB and inflammatory response, increased in lesions while three cell cycle-related gene sets, MYC targets, G2M checkpoint, and E2F targets were decreased. This indicates increased inflammation and decreased proliferation in lesions compared to eutopic endometrium.

Tables

Table 1

Patient demographics, indications for surgery, and post-operative diagnosis.

Patient	Age	Indication(s)	Diagnosis
2756	47	Uterine Leiomyoma Adenomyosis	Endometriosis L ovary and oviduct
4909	36	Uterine Leiomyoma Pelvic pain	Endometriosis, Leiomyoma
5322	49	Uterine Leiomyoma	Endometriosis L&R ovary, Leiomyoma
9997	36	Pelvic pain	Endometriosis R oviduct, Endometrioma L ovary, Pelvic adhesions
12529	44	Uterine Leiomyoma	Endometriosis L&R oviduct, Leiomyoma

597 # References

598 1. Eskenazi B, Warner ML. Epidemiology of endometriosis. Obstet Gynecol Clin North Am.
599 1997;24(2):235-58. Epub 1997/06/01. PubMed PMID: 9163765.
600 2. Bulun SE. Endometriosis. N Engl J Med. 2009;360(3):268-79. Epub 2009/01/16. doi:
601 10.1056/NEJMra0804690. PubMed PMID: 19144942.
602 3. Giudice LC. Clinical practice. Endometriosis. N Engl J Med. 2010;362(25):2389-98. Epub
603 2010/06/25. doi: 10.1056/NEJMcp1000274. PubMed PMID: 20573927; PubMed Central
604 PMCID: PMCPMC3108065.
605 4. Practice Committee of the American Society for Reproductive Medicine. Treatment of pelvic
606 pain associated with endometriosis. Fertil Steril. 2008;90(5 Suppl):S260-9. Epub 2008/11/26.
607 doi: 10.1016/j.fertnstert.2008.08.057. PubMed PMID: 19007642.
608 5. Endometriosis and infertility: a committee opinion. Fertil Steril. 2012;98(3):591-8. Epub
609 2012/06/19. doi: 10.1016/j.fertnstert.2012.05.031. PubMed PMID: 22704630.
610 6. Koninckx PR, Martin DC. Deep endometriosis: a consequence of infiltration or retraction or
611 possibly adenomyosis externa? Fertil Steril. 1992;58(5):924-8. Epub 1992/11/01. doi:
612 10.1016/s0015-0282(16)55436-3. PubMed PMID: 1426377.
613 7. Koninckx PR, Ussia A, Adamyan L, Wattiez A, Donnez J. Deep endometriosis: definition,
614 diagnosis, and treatment. Fertil Steril. 2012;98(3):564-71. Epub 2012/09/04. doi:
615 10.1016/j.fertnstert.2012.07.1061. PubMed PMID: 22938769.
616 8. Sampson JA. Peritoneal endometriosis due to the menstrual dissemination of endometrial
617 tissue into the peritoneal cavity. American Journal of Obstetrics & Gynecology.
618 1927;14(4):422-69. doi: 10.1016/S0002-9378(15)30003-X.
619 9. Zondervan KT, Becker CM, Koga K, Missmer SA, Taylor RN, Vigano P. Endometriosis. Nat
620 Rev Dis Primers. 2018;4(1):9. Epub 2018/07/22. doi: 10.1038/s41572-018-0008-5. PubMed
621 PMID: 30026507.
622 10. Hastings JM, Fazleabas AT. A baboon model for endometriosis: implications for fertility.
623 Reprod Biol Endocrinol. 2006;4 Suppl 1:S7. Epub 2006/11/23. doi: 10.1186/1477-7827-4-S1-
624 S7. PubMed PMID: 17118171; PubMed Central PMCID: PMCPMC1775067.
625 11. Jones CJ, Denton J, Fazleabas AT. Morphological and glycosylation changes associated with
626 the endometrium and ectopic lesions in a baboon model of endometriosis. Hum Reprod.
627 2006;21(12):3068-80. Epub 2006/10/05. doi: 10.1093/humrep/del310. PubMed PMID:
628 17018533.

12. Harirchian P, Gashaw I, Lipskind ST, Braundmeier AG, Hastings JM, Olson MR, et al. Lesion kinetics in a non-human primate model of endometriosis. Hum Reprod. 2012;27(8):2341-51. Epub 2012/06/08. doi: 10.1093/humrep/des196. PubMed PMID: 22674203; PubMed Central PMCID: PMCPMC3398680.
13. Greaves E, Cousins FL, Murray A, Esnal-Zufiaurre A, Fassbender A, Horne AW, et al. A novel mouse model of endometriosis mimics human phenotype and reveals insights into the inflammatory contribution of shed endometrium. Am J Pathol. 2014;184(7):1930-9. Epub 2014/06/10. doi: 10.1016/j.ajpath.2014.03.011. PubMed PMID: 24910298; PubMed Central PMCID: PMCPMC4076466.
14. Dorning A, Dhami P, Panir K, Hogg C, Park E, Ferguson GD, et al. Bioluminescent imaging in induced mouse models of endometriosis reveals differences in four model variations. Dis Model Mech. 2021;14(8). Epub 2021/08/13. doi: 10.1242/dmm.049070. PubMed PMID: 34382636; PubMed Central PMCID: PMCPMC8419713.
15. Vigano P, Ottolina J, Bartiromo L, Bonavina G, Schimberni M, Villanacci R, et al. Cellular Components Contributing to Fibrosis in Endometriosis: A Literature Review. J Minim Invasive Gynecol. 2020;27(2):287-95. Epub 2019/12/01. doi: 10.1016/j.jmig.2019.11.011. PubMed PMID: 31785417.
16. Vigano P, Candiani M, Monno A, Giacomini E, Vercellini P, Somigliana E. Time to redefine endometriosis including its pro-fibrotic nature. Hum Reprod. 2018;33(3):347-52. Epub 2017/12/06. doi: 10.1093/humrep/dex354. PubMed PMID: 29206943.
17. Brosens I, Puttemans P, Benagiano G. Which cell defines endometriosis? Hum Reprod. 2018;33(3):357-60. Epub 2018/02/09. doi: 10.1093/humrep/dey016. PubMed PMID: 29420768.
18. Capobianco A, Rovere-Querini P. Endometriosis, a disease of the macrophage. Front Immunol. 2013;4:9. Epub 2013/02/02. doi: 10.3389/fimmu.2013.00009. PubMed PMID: 23372570; PubMed Central PMCID: PMCPMC3556586.
19. Song Y, Burns GW, Joshi NR, Arora R, Kim JJ, Fazleabas AT. Spheroids as a model for endometriotic lesions. JCI Insight. 2023;8(11). Epub 2023/04/27. doi: 10.1172/jci.insight.160815. PubMed PMID: 37104033.
20. Marla S, Mortlock S, Heinosalo T, Poutanen M, Montgomery GW, McKinnon BD. Gene expression profiles separate endometriosis lesion subtypes and indicate a sensitivity of endometrioma to estrogen suppressive treatments through elevated ESR2 expression. BMC Med. 2023;21(1):460. Epub 2023/11/24. doi: 10.1186/s12916-023-03166-1. PubMed PMID: 37996888; PubMed Central PMCID: PMCPMC10666321.

663 21. Tan Y, Flynn WF, Sivajothi S, Luo D, Bozal SB, Davé M, et al. Single-cell analysis of
664 endometriosis reveals a coordinated transcriptional programme driving immunotolerance and
665 angiogenesis across eutopic and ectopic tissues. Nat Cell Biol. 2022. Epub 2022/07/22. doi:
666 10.1038/s41556-022-00961-5. PubMed PMID: 35864314.
667 22. Fonseca MAS, Haro M, Wright KN, Lin X, Abbasi F, Sun J, et al. Single-cell transcriptomic
668 analysis of endometriosis. Nat Genet. 2023;55(2):255-67. Epub 2023/01/10. doi:
669 10.1038/s41588-022-01254-1. PubMed PMID: 36624343.
670 23. Li R, Tran DN, Lessey BA, Young SL, Kim TH, Jeong JW. Transcriptomic changes in eutopic
671 endometrium and ectopic lesions during endometriosis progression in a mouse model. F S
672 Sci. 2024. Epub 2024/02/12. doi: 10.1016/j.xfss.2024.02.001. PubMed PMID: 38342342.
673 24. Zollinger DR, Lingle SE, Sorg K, Beechem JM, Merritt CR. GeoMx™ RNA Assay: High
674 Multiplex, Digital, Spatial Analysis of RNA in FFPE Tissue. Methods in molecular biology.
675 2020;2148:331-45. Epub 2020/05/13. doi: 10.1007/978-1-0716-0623-0_21. PubMed PMID:
676 32394392.
677 25. Blumhagen RZ, Kurche JS, Cool CD, Walts AD, Heinz D, Fingerlin TE, et al. Spatially distinct
678 molecular patterns of gene expression in idiopathic pulmonary fibrosis. Respir Res.
679 2023;24(1):287. Epub 2023/11/18. doi: 10.1186/s12931-023-02572-6. PubMed PMID:
680 37978501; PubMed Central PMCID: PMCPMC10655274.
681 26. Pennel KAF, Hatthakarnkul P, Wood CS, Lian GY, Al-Badran SSF, Quinn JA, et al. JAK/STAT3
682 represents a therapeutic target for colorectal cancer patients with stromal-rich tumors. J Exp
683 Clin Cancer Res. 2024;43(1):64. Epub 2024/03/01. doi: 10.1186/s13046-024-02958-4.
684 PubMed PMID: 38424636; PubMed Central PMCID: PMCPMC10905886.
685 27. Liberzon A, Birger C, Thorvaldsdóttir H, Ghandi M, Mesirov JP, Tamayo P. The Molecular
686 Signatures Database (MSigDB) hallmark gene set collection. Cell Syst. 2015;1(6):417-25.
687 Epub 2016/01/16. doi: 10.1016/j.cels.2015.12.004. PubMed PMID: 26771021; PubMed
688 Central PMCID: PMCPMC4707969.
689 28. Subramanian A, Tamayo P, Mootha VK, Mukherjee S, Ebert BL, Gillette MA, et al. Gene set
690 enrichment analysis: a knowledge-based approach for interpreting genome-wide expression
691 profiles. Proc Natl Acad Sci U S A. 2005;102(43):15545-50. Epub 2005/10/04. doi:
692 10.1073/pnas.0506580102. PubMed PMID: 16199517; PubMed Central PMCID:
693 PMCPMC1239896.
694 29. Jin S, Guerrero-Juarez CF, Zhang L, Chang I, Ramos R, Kuan CH, et al. Inference and
695 analysis of cell-cell communication using CellChat. Nat Commun. 2021;12(1):1088. Epub

696 2021/02/19. doi: 10.1038/s41467-021-21246-9. PubMed PMID: 33597522; PubMed Central
697 PMCID: PMCPMC7889871.
698 30. Harada T, Iwabe T, Terakawa N. Role of cytokines in endometriosis. Fertility and Sterility.
699 2001;76(1):1-10. doi: https://doi.org/10.1016/S0015-0282(01)01816-7.
700 31. Noble LS, Simpson ER, Johns A, Bulun SE. Aromatase expression in endometriosis. J Clin
701 Endocrinol Metab. 1996;81(1):174-9. Epub 1996/01/01. doi: 10.1210/jcem.81.1.8550748.
702 PubMed PMID: 8550748.
703 32. Attia GR, Zeitoun K, Edwards D, Johns A, Carr BR, Bulun SE. Progesterone receptor isoform
704 A but not B is expressed in endometriosis. J Clin Endocrinol Metab. 2000;85(8):2897-902.
705 Epub 2000/08/18. doi: 10.1210/jcem.85.8.6739. PubMed PMID: 10946900.
706 33. Bulun SE, Yang S, Fang Z, Gurates B, Tamura M, Sebastian S. Estrogen production and
707 metabolism in endometriosis. Annals of the New York Academy of Sciences. 2002;955:75-85;
708 discussion 6-8, 396-406. Epub 2002/04/13. doi: 10.1111/j.1749-6632.2002.tb02767.x.
709 PubMed PMID: 11949967.
710 34. Fazleabas AT, Brudney A, Chai D, Langoi D, Bulun SE. Steroid receptor and aromatase
711 expression in baboon endometriotic lesions. Fertil Steril. 2003;80 Suppl 2:820-7. Epub
712 2003/09/25. doi: 10.1016/s0015-0282(03)00982-8. PubMed PMID: 14505759.
713 35. Attar E, Tokunaga H, Imir G, Yilmaz MB, Redwine D, Putman M, et al. Prostaglandin E2 via
714 steroidogenic factor-1 coordinately regulates transcription of steroidogenic genes necessary
715 for estrogen synthesis in endometriosis. J Clin Endocrinol Metab. 2009;94(2):623-31. Epub
716 2008/11/13. doi: 10.1210/jc.2008-1180. PubMed PMID: 19001523; PubMed Central PMCID:
717 PMCPMC2646521.
718 36. Yilmaz BD, Bulun SE. Endometriosis and nuclear receptors. Hum Reprod Update.
719 2019;25(4):473-85. doi: 10.1093/humupd/dmz005. PubMed Central PMCID:
720 PMCPMC6601390.
721 37. Ohlsson Teague EM, Van der Hoek KH, Van der Hoek MB, Perry N, Wagaarachchi P,
722 Robertson SA, et al. MicroRNA-regulated pathways associated with endometriosis. Mol
723 Endocrinol. 2009;23(2):265-75. Epub 2008/12/17. doi: 10.1210/me.2008-0387. PubMed
724 PMID: 19074548; PubMed Central PMCID: PMCPMC5419313.
725 38. Nothnick WB, Falcone T, Joshi N, Fazleabas AT, Graham A. Serum miR-451a Levels Are
726 Significantly Elevated in Women With Endometriosis and Recapitulated in Baboons (Papio
727 anubis) With Experimentally-Induced Disease. Reproductive sciences (Thousand Oaks,
728 Calif). 2017;24(8):1195-202. Epub 2016/12/07. doi: 10.1177/1933719116681519. PubMed
729 PMID: 27920341.

730 39. Rekker K, Tasa T, Saare M, Samuel K, Kadastik U, Karro H, et al. Differentially-Expressed
731 miRNAs in Ectopic Stromal Cells Contribute to Endometriosis Development: The Plausible
732 Role of miR-139-5p and miR-375. Int J Mol Sci. 2018;19(12). Epub 2018/11/30. doi:
733 10.3390/ijms19123789. PubMed PMID: 30487429; PubMed Central PMCID:
734 PMCPMC6321240.
735 40. Pavone ME, Grover AR, Confino R, Pearson EK, Malpani S, Cheng YH, et al. Retinoic acid
736 action is altered within endometrium of baboons affected with endometriosis. Journal of
737 Endometriosis and Pelvic Pain Disorders. 2022:22840265211062008. doi:
738 10.1177/22840265211062008. PubMed PMID: WOS:000740968400001.
739 41. Song Y, Su RW, Joshi NR, Kim TH, Lessey BA, Jeong JW, et al. Interleukin-6 (IL-6) Activates
740 the NOTCH1 Signaling Pathway Through E-Proteins in Endometriotic Lesions. J Clin
741 Endocrinol Metab. 2020;105(5). Epub 2020/03/03. doi: 10.1210/clinem/dgaa096. PubMed
742 PMID: 32119078; PubMed Central PMCID: PMCPMC7096313.
743 42. Kai K, Joshi NR, Burns GW, Hrbek SM, Vegter EL, Ochoa-Bernal MA, et al. MicroRNA-210-
744 3p Regulates Endometriotic Lesion Development by Targeting IGFBP3 in Baboons and
745 Women with Endometriosis. Reproductive sciences (Thousand Oaks, Calif).
746 2023;30(10):2932-44. Epub 2023/05/16. doi: 10.1007/s43032-023-01253-5. PubMed PMID:
747 37188982; PubMed Central PMCID: PMCPMC10556147.
748 43. Hogg C, Panir K, Dhami P, Rosser M, Mack M, Soong D, et al. Macrophages inhibit and
749 enhance endometriosis depending on their origin. Proc Natl Acad Sci U S A. 2021;118(6).
750 Epub 2021/02/05. doi: 10.1073/pnas.2013776118. PubMed PMID: 33536334.
751 44. Hogg C, Horne AW, Greaves E. Endometriosis-Associated Macrophages: Origin, Phenotype,
752 and Function. Front Endocrinol (Lausanne). 2020;11:7. Epub 2020/02/11. doi:
753 10.3389/fendo.2020.00007. PubMed PMID: 32038499; PubMed Central PMCID:
754 PMCPMC6989423.
755 45. Henlon Y, Panir K, McIntyre I, Hogg C, Dhami P, Cuff AO, et al. Single-cell analysis identifies
756 distinct macrophage phenotypes associated with pro-disease and pro-resolving functions in
757 the endometriotic niche. bioRxiv. 2024:2024.03.07.583861. doi: 10.1101/2024.03.07.583861.
758 46. Croasdell Lucchini A, Gachanja NN, Rossi AG, Dorward DA, Lucas CD. Epithelial Cells and
759 Inflammation in Pulmonary Wound Repair. Cells. 2021;10(2). Epub 2021/02/11. doi:
760 10.3390/cells10020339. PubMed PMID: 33562816; PubMed Central PMCID:
761 PMCPMC7914803.

762 47. Ren JL, Pan JS, Lu YP, Sun P, Han J. Inflammatory signaling and cellular senescence. Cell
763 Signal. 2009;21(3):378-83. Epub 2008/11/11. doi: 10.1016/j.cellsig.2008.10.011. PubMed
764 PMID: 18992324; PubMed Central PMCID: PMCPMC2870712.
765 48. Zou L, Meng L, Xu Y, Wang K, Zhang J. Revealing the diagnostic value and immune infiltration
766 of senescence-related genes in endometriosis: a combined single-cell and machine learning
767 analysis. Front Pharmacol. 2023;14:1259467. Epub 2023/10/20. doi:
768 10.3389/fphar.2023.1259467. PubMed PMID: 37860112; PubMed Central PMCID:
769 PMCPMC10583561.
770 49. Muter J, Kong CS, Brosens JJ. The Role of Decidual Subpopulations in Implantation,
771 Menstruation and Miscarriage. Front Reprod Health. 2021;3:804921. Epub 2022/10/29. doi:
772 10.3389/frph.2021.804921. PubMed PMID: 36303960; PubMed Central PMCID:
773 PMCPMC9580781.
774 50. Crocker PR, Jefferies WA, Clark SJ, Chung LP, Gordon S. Species heterogeneity in
775 macrophage expression of the CD4 antigen. J Exp Med. 1987;166(2):613-8. Epub
776 1987/08/01. doi: 10.1084/jem.166.2.613. PubMed PMID: 3110358; PubMed Central PMCID:
777 PMCPMC2189597.
778 51. Zhen A, Krutzik SR, Levin BR, Kasparian S, Zack JA, Kitchen SG. CD4 ligation on human
779 blood monocytes triggers macrophage differentiation and enhances HIV infection. J Virol.
780 2014;88(17):9934-46. Epub 2014/06/20. doi: 10.1128/jvi.00616-14. PubMed PMID:
781 24942581; PubMed Central PMCID: PMCPMC4136363.
782 52. Stevenson M. HIV-1 pathogenesis. Nat Med. 2003;9(7):853-60. Epub 2003/07/02. doi:
783 10.1038/nm0703-853. PubMed PMID: 12835705.
784 53. Betjes MG, Haks MC, Tuk CW, Beelen RH. Monoclonal antibody EBM11 (anti-CD68)
785 discriminates between dendritic cells and macrophages after short-term culture.
786 Immunobiology. 1991;183(1-2):79-87. Epub 1991/09/01. doi: 10.1016/s0171-2985(11)80187-
787 7. PubMed PMID: 1834546.
788 54. Yan J, Zhou L, Liu M, Zhu H, Zhang X, Cai E, et al. Single-cell analysis reveals insights into
789 epithelial abnormalities in ovarian endometriosis. Cell Rep. 2024;43(3):113716. Epub
790 2024/02/27. doi: 10.1016/j.celrep.2024.113716. PubMed PMID: 38412094.
791 55. Calandra T, Roger T. Macrophage migration inhibitory factor: a regulator of innate immunity.
792 Nat Rev Immunol. 2003;3(10):791-800. Epub 2003/09/23. doi: 10.1038/nri1200. PubMed
793 PMID: 14502271; PubMed Central PMCID: PMCPMC7097468.
794 56. Mitchell RA, Metz CN, Peng T, Bucala R. Sustained mitogen-activated protein kinase (MAPK)
795 and cytoplasmic phospholipase A2 activation by macrophage migration inhibitory factor (MIF).

796 Regulatory role in cell proliferation and glucocorticoid action. J Biol Chem.
797 1999;274(25):18100-6. Epub 1999/06/11. doi: 10.1074/jbc.274.25.18100. PubMed PMID:
798 10364264.
799 57. Schenkein HA, Rutherford B. C3-mediated release of prostaglandin from human monocytes.
800 Behaviour in short-term culture. Immunology. 1984;51(1):83-91. Epub 1984/01/01. PubMed
801 PMID: 6690398; PubMed Central PMCID: PMCPMC1454415.
802 58. Calandra T, Bernhagen J, Mitchell RA, Bucala R. The macrophage is an important and
803 previously unrecognized source of macrophage migration inhibitory factor. J Exp Med.
804 1994;179(6):1895-902. Epub 1994/06/01. doi: 10.1084/jem.179.6.1895. PubMed PMID:
805 8195715; PubMed Central PMCID: PMCPMC2191507.
806 59. Bacher M, Metz CN, Calandra T, Mayer K, Chesney J, Lohoff M, et al. An essential regulatory
807 role for macrophage migration inhibitory factor in T-cell activation. Proc Natl Acad Sci U S A.
808 1996;93(15):7849-54. Epub 1996/07/23. doi: 10.1073/pnas.93.15.7849. PubMed PMID:
809 8755565; PubMed Central PMCID: PMCPMC38837.
810 60. Weed JC, Arquembourg PC. Endometriosis: can it produce an autoimmune response
811 resulting in infertility? Clin Obstet Gynecol. 1980;23(3):885-93. Epub 1980/09/01. PubMed
812 PMID: 7418287.
813 61. Isaacson KB, Coutifaris C, Garcia CR, Lyttle CR. Production and secretion of complement
814 component 3 by endometriotic tissue. J Clin Endocrinol Metab. 1989;69(5):1003-9. Epub
815 1989/11/01. doi: 10.1210/jcem-69-5-1003. PubMed PMID: 2793987.
816 62. Tao XJ, Sayegh RA, Isaacson KB. Increased expression of complement component 3 in
817 human ectopic endometrium compared with the matched eutopic endometrium. Fertil Steril.
818 1997;68(3):460-7. Epub 1997/10/07. doi: 10.1016/s0015-0282(97)00254-9. PubMed PMID:
819 9314915.
820 63. Hasan A, Rahim A, Afzal M, Naveed AK, Ayub S, Jahan S. Serum Albumin and C3
821 Complement Levels in Endometriosis. J Coll Physicians Surg Pak. 2019;29(8):702-5. Epub
822 2019/07/31. doi: 10.29271/jcpsp.2019.08.702. PubMed PMID: 31358086.
823 64. Young SL. The complement system and its role in the endometrium. In: Aplin JD, Fazleabas
824 AT, Glasser SR, Giudice LC, editors. The Endometrium: Molecular, Cellular and Clinical
825 Perspectives, Second Edition: Taylor & Francis; 2008. p. 568-78.
826 65. Agostinis C, Balduit A, Mangogna A, Zito G, Romano F, Ricci G, et al. Immunological Basis of
827 the Endometriosis: The Complement System as a Potential Therapeutic Target. Front
828 Immunol. 2020;11:599117. Epub 2021/01/29. doi: 10.3389/fimmu.2020.599117. PubMed
829 PMID: 33505394; PubMed Central PMCID: PMCPMC7829336.

830 66. Brown EJ, Frazier WA. Integrin-associated protein (CD47) and its ligands. Trends Cell Biol.
831 2001;11(3):130-5. Epub 2001/04/18. doi: 10.1016/s0962-8924(00)01906-1. PubMed PMID:
832 11306274.
833 67. Gresham HD, Dale BM, Potter JW, Chang PW, Vines CM, Lowell CA, et al. Negative
834 regulation of phagocytosis in murine macrophages by the Src kinase family member, Fgr. J
835 Exp Med. 2000;191(3):515-28. Epub 2000/02/09. doi: 10.1084/jem.191.3.515. PubMed
836 PMID: 10662797; PubMed Central PMCID: PMCPMC2195814.
837 68. Meri S, Morgan BP, Davies A, Daniels RH, Olavesen MG, Waldmann H, et al. Human protectin
838 (CD59), an 18,000-20,000 MW complement lysis restricting factor, inhibits C5b-8 catalysed
839 insertion of C9 into lipid bilayers. Immunology. 1990;71(1):1-9. Epub 1990/09/01. PubMed
840 PMID: 1698710; PubMed Central PMCID: PMCPMC1384213.
841 69. Yang H, Li L, Liu X, Zhao Y. High Expression of the Component 3a Receptor 1 (C3AR1) Gene
842 in Stomach Adenocarcinomas Infers a Poor Prognosis and High Immune-Infiltration Levels.
843 Med Sci Monit. 2021;27:e927977. Epub 2021/02/05. doi: 10.12659/msm.927977. PubMed
844 PMID: 33539329; PubMed Central PMCID: PMCPMC7871482.
845 70. Zhu S, Wang A, Xu W, Hu L, Sun J, Wang X. The heterogeneity of fibrosis and angiogenesis
846 in endometriosis revealed by single-cell RNA-sequencing. Biochim Biophys Acta Mol Basis
847 Dis. 2023;1869(2):166602. Epub 2022/11/19. doi: 10.1016/j.bbadis.2022.166602. PubMed
848 PMID: 36400338.
849 71. Sunderkötter C, Steinbrink K, Goebeler M, Bhardwaj R, Sorg C. Macrophages and
850 angiogenesis. J Leukoc Biol. 1994;55(3):410-22. Epub 1994/03/01. doi: 10.1002/jlb.55.3.410.
851 PubMed PMID: 7509844.
852 72. Martínez-Ramos S, Rafael-Vidal C, Malvar-Fernández B, Pérez N, Mouriño C, Pérez SG, et
853 al. Semaphorin3B promotes an anti-inflammatory and pro-resolving phenotype in
854 macrophages from rheumatoid arthritis patients in a MerTK-dependent manner. Front
855 Immunol. 2023;14:1268144. Epub 2024/01/29. doi: 10.3389/fimmu.2023.1268144. PubMed
856 PMID: 38283352; PubMed Central PMCID: PMCPMC10811190.
857 73. Bulun SE, Fang Z, Imir G, Gurates B, Tamura M, Yilmaz B, et al. Aromatase and
858 endometriosis. Semin Reprod Med. 2004;22(1):45-50. Epub 2004/04/15. doi: 10.1055/s-
859 2004-823026. PubMed PMID: 15083380.
860 74. Ullah K, Rahman TU, Pan HT, Guo MX, Dong XY, Liu J, et al. Serum estradiol levels in
861 controlled ovarian stimulation directly affect the endometrium. J Mol Endocrinol.
862 2017;59(2):105-19. Epub 2017/05/26. doi: 10.1530/jme-17-0036. PubMed PMID: 28539318;
863 PubMed Central PMCID: PMCPMC5510595.

75. Agostinis C, Zorzet S, Balduit A, Zito G, Mangogna A, Macor P, et al. The Inflammatory Feed-Forward Loop Triggered by the Complement Component C3 as a Potential Target in Endometriosis. Front Immunol. 2021;12:693118. Epub 2021/09/08. doi: 10.3389/fimmu.2021.693118. PubMed PMID: 34489939; PubMed Central PMCID: PMCPMC8418148.
76. Ruiz LA, Baez-Vega PM, Ruiz A, Peterse DP, Monteiro JB, Bracero N, et al. Dysregulation of Lysyl Oxidase Expression in Lesions and Endometrium of Women With Endometriosis. Reproductive sciences (Thousand Oaks, Calif). 2015;22(12):1496-508. Epub 2015/05/13. doi: 10.1177/1933719115585144. PubMed PMID: 25963914; PubMed Central PMCID: PMCPMC5933196.
77. Colon-Diaz M, Baez-Vega P, Garcia M, Ruiz A, Monteiro JB, Fourquet J, et al. HDAC1 and HDAC2 are differentially expressed in endometriosis. Reproductive sciences (Thousand Oaks, Calif). 2012;19(5):483-92. Epub 2012/02/22. doi: 10.1177/1933719111432870. PubMed PMID: 22344732; PubMed Central PMCID: PMCPMC3343094 research, authorship, and/or publication of this article.
78. Colón-Caraballo M, García M, Mendoza A, Flores I. Human Endometriosis Tissue Microarray Reveals Site-specific Expression of Estrogen Receptors, Progesterone Receptor, and Ki67. Appl Immunohistochem Mol Morphol. 2019;27(7):491-500. Epub 2018/04/10. doi: 10.1097/pai.0000000000000663. PubMed PMID: 29629944; PubMed Central PMCID: PMCPMC6174114.
79. Noyes RW, Hertig AT, Rock J. Dating the endometrial biopsy. American journal of obstetrics and gynecology. 1975;122(2):262-3. Epub 1975/05/01. doi: 10.1016/s0002-9378(16)33500-1. PubMed PMID: 1155504.
80. McInnes L, Healy J, Melville J. Umap: Uniform manifold approximation and projection for dimension reduction. arXiv preprint arXiv:180203426. 2018.
81. Ritchie ME, Phipson B, Wu D, Hu Y, Law CW, Shi W, et al. limma powers differential expression analyses for RNA-sequencing and microarray studies. Nucleic Acids Res. 2015;43(7):e47. Epub 2015/01/22. doi: 10.1093/nar/gkv007. PubMed PMID: 25605792; PubMed Central PMCID: PMCPMC4402510.
82. Schneider CA, Rasband WS, Eliceiri KW. NIH Image to ImageJ: 25 years of image analysis. Nat Methods. 2012;9(7):671-5. Epub 2012/08/30. doi: 10.1038/nmeth.2089. PubMed PMID: 22930834; PubMed Central PMCID: PMCPMC5554542.
83. Team R. RStudio: Integrated Development for R. Boston, MA: RStudio, PBC.; 2020. Available from: http://www.rstudio.com/.

898 84. McCarthy DJ, Chen Y, Smyth GK. Differential expression analysis of multifactor RNA-Seq
899 experiments with respect to biological variation. Nucleic Acids Res. 2012;40(10):4288-97.
900 Epub 2012/01/31. doi: 10.1093/nar/gks042. PubMed PMID: 22287627; PubMed Central
901 PMCID: PMCPMC3378882.
902 85. Zhou X, Lindsay H, Robinson MD. Robustly detecting differential expression in RNA
903 sequencing data using observation weights. Nucleic Acids Res. 2014;42(11):e91. Epub
904 2014/04/23. doi: 10.1093/nar/gku310. PubMed PMID: 24753412; PubMed Central PMCID:
905 PMCPMC4066750.
906 86. Wu T, Hu E, Xu S, Chen M, Guo P, Dai Z, et al. clusterProfiler 4.0: A universal enrichment tool
907 for interpreting omics data. Innovation (Camb). 2021;2(3):100141. Epub 2021/09/25. doi:
908 10.1016/j.xinn.2021.100141. PubMed PMID: 34557778; PubMed Central PMCID:
909 PMCPMC8454663.
910